2011

Development of High Sensitivity Spectral Fiber Polarimeter for Protein Investigations

Maryam Gouran Orimi

Development of High Sensitivity Spectral Fiber Polarimeter for Protein Investigations

(Spine title: Development of Spectral Polarimeter)

(Thesis Format: Monograph)

by

Maryam Gouran Orimi

Graduate Program in Biomedical Engineering

A thesis submitted in partial fulfillment

of the requirements for the degree of

Master of Science

School of Graduate and Postdoctoral Studies

The University of Western Ontario

London, Ontario, Canada

THE UNIVERSITY OF WESTERN ONTARIO
SCHOOL OF GRADUATE AND POSTDOCTORAL STUDIES

CERTIFICATE OF EXAMINATION

Supervisor	Examiners
Dr. Silvia Mittler	Dr. Jayshri Sabarinathan
Advisory Committee	Dr. Argyrios Margaritis
Dr. Amin Rizkalla	Dr. Ian Cunningham
Dr. Jayshri Sabarinathan	

The thesis by

Maryam Gouran Orimi

entitled:

Development of High Sensitivity Spectral Fiber Polarimeter for Protein Investigations

is accepted in partial fulfillment of the
requirements for the degree of
Master of Science

Date_____

_____
Chair of the Thesis Examination Board

Abstract

Proteins are essential ingredients of every living cell and organism and display a special property called optical activity, meaning their ability to turn the polarization direction of linearly polarized light in a very particular fashion. The magnitude of this polarization turning angle depends on the nature of the amino acid side chain. The temperature, the wavelength of the light used in the measurement, the specific optical activity of the molecule, the concentration and the interaction length of the light beam applied through the specimen can also affect optical rotation behavior. In previous work, a simple laser fiber polarimeter based on a liquid-core silica hollow optical fiber waveguide with an extremely small volume (39 µl) but a light interaction length of 2.2 m was bulit to investigate the optical activity of chiral molecules. In this thesis the fundamental liquid-core fibre polarimeter setup was employed to test and characterize fused silica and teflon AF fibres in different lengths and it was proved that the fibre length for the silica and Teflon AF fibre could be extended up to 5 and 2 m, respectively. Clearly path length is the most important advantage of this polarimeter which led to development of a new spectral polarimeter system to take advantage of the optical rotatory dispersion of chiral molecules e.g. proteins. This new setup has been built and in order to gain the best efficiency from the spectral polarimeter setup and optimize the function of it, the setup was characterized and optimized in three parts: the light source, temperaure stabilized box and the detection system. To prove the spectral fibrer polarimeter works properly and shows an improvement due to the enhanced sample interaction length, the polarimeter was tested with a chiral material in different concentrations and fibre length. A detection resolution in order of microdegrees and a

limit of detection (LOD) of 0.3 and 0.1 μM for a 220.4 and 428.8 cm fiber were found with this new spectral polarimeter which confirmed the enhancement of sensitivity. The optical rotation changes in collagen solution were invetigated by this new technology.

Keywords: proteins, optical activity, spectral polarimeter, hollow optical fiber, enhancement of sensitivity

Acknowledgements

I would like to express my gratitude to all those who gave me the possibility to complete this thesis. I am deeply grateful to my supervisor, Dr. S. Mittler whose help, stimulating suggestions and encouragement helped me in all the time of research and writing of this thesis. Besides my supervisor, I would like to thank the rest of my thesis committee: Dr. J. Sabarinathan and Dr. A. Rizkalla for their encouragement, insightful comments, and hard questions.

I am indebted to my many of my colleagues to support me in my research work. I want to thank them for all their help, support, interest and valuable hints. I am grateful to all my friends for being the surrogate family during these years and for their continued moral support. The most special thanks goes to my family whose patient love enabled me to complete this work.

TABLE OF CONTENTS

LIST OF TABLES

LIST OF FIGURES

LIST OF ABBREVIATIONS AND UNITS

CD: Circular Dichroism

ORD: Optical rotatory dispersion

LD: Limit of Detection

PMD: Polarization Mode Dispersion

PDL: Polarization Dependent Loss

PMT: Photo Multiplier Tube

RAF: Righ Angle Figuration

$[\alpha]_{\lambda}$: specific rotation deg cm^2 g^{-1}

$[m]_{\lambda}$: molar rotation deg cm^2 mol^{-1}

$[m']_{\lambda}$: reduced mean residue rotation deg cm^2 mol^{-1}

CHAPTER 1
LITERATURE REVIEW

1.1. Introduction

Proteins are large molecules composed of one or more chains of amino acids in a specific order. The order is determined by the base sequence of nucleotides in the gene that codes for the protein. Proteins are required for the structure, function, and regulation of the body's cells, tissues, and organs and include many substances, such as enzymes, hormones, and antibodies, and each of them has unique functions [1]. Proteins are defined as linear chains of amino acids that adopt a unique three-dimensional structure in their native surroundings [2].The three-dimensional structure of a protein defines not only its size and shape, but also its function [3]. Thus in order to understand the details of protein function, we must understand their structure [4]. Protein structures generally are described at four levels (fig.1.1). The primary structure of each protein is described by the specific amino acid sequences, encoded by the mRNA, which directs the proper folding of the polypeptide chain into the secondary structure. The most common types of secondary structure in the proteins are the α-helices and the β-sheets. The α-helix is a region of the polypeptide that folds into a corkscrew shape. A β-sheet consists of two or more hydrogen bonded β-strands forming a sheet like structure. Other regions of secondary structure may include turns and random coils. These helices, sheets, turns, and coils interact chemically with each other to form the unique three-dimensional shape of the protein, called the tertiary structure. Tertiary structure is the global folding of a single polypeptide chain. Many proteins, however, have several different polypeptide subunits that make the final active protein. For these proteins, interactions between the different subunits form the quaternary structure [3].

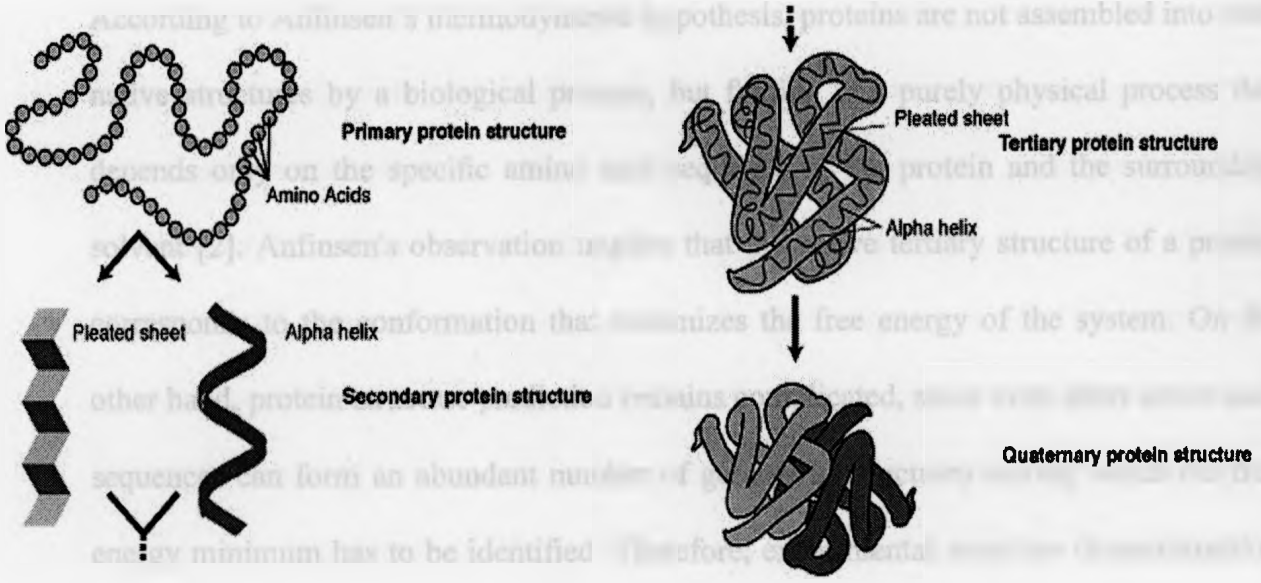

Figure 1.1. *Protein Structure, from primary to quaternary (Adopted from [5])*

1.2. Protein Structure Prediction

The protein structure prediction has attracted the interest of many researchers across several disciplines [6]. There are several viewpoints regarding to the protein folding question. The classical one considers the folding as a hierarchical process, implying that the process begins by rapid formation of secondary structural elements, and the formation of native secondary structure precedes the formation of tertiary interactions as well [7]. The opposing view is based on the idea of a hydrophobic collapse that suggests the tertiary and secondary features form simultaneously. There is also another viewpoint that combines the components of the mentioned ones. It describes that (a) local interactions form helices and beta strands, (b) hydrophobic long range interactions are responsible for the formation of beta-sheets and their topologies, and (c) the combination of the results from (a) and (b) drive the protein into its folded structure [8,9].

According to Anfinsen's thermodynamic hypothesis, proteins are not assembled into their native structures by a biological process, but folding is a purely physical process that depends only on the specific amino acid sequence of the protein and the surrounding solvent [2]. Anfinsen's observation implies that the native tertiary structure of a protein corresponds to the conformation that minimizes the free energy of the system. On the other hand, protein structure prediction remains complicated, since even short amino acid sequences can form an abundant number of geometric structures among which the free energy minimum has to be identified. Therefore, experimental structure characterization is a major and extremely important issue in protein structure-function relationship research. The number of protein structures that have been determined experimentally continues to grow rapidly [8]. There is a variety of experimental technology to determine the primary, secondary and tertiary structure and changes in them. Though several methods exist to sequence proteins primary structure, the two dominant methods are Mass Spectrometry [10] and Edman Degradation [11]. The secondary structures are often investigated with CD-spectroscopy [12]. Most tertiary structures have been found by x-ray crystallography, NMR spectroscopy, and dual polarization interferometry [13]. Polarimetry in the UV and visible spectral regime are other methods used rarely to determine secondary and tertiary structures of proteins and conformational changes in them [14].

1.3. Chirality and Optical Activity in Proteins

The chirality of protein amino acids is a universal phenomenon observed in organisms from all the kingdoms. Indeed, such universality has been referred as the first

principle of biochemistry [15]. The base of chirality in biology (protein amino acids, sugars in nucleic acids, and lecithins in the cellular plasma membrane) are not well understood, in spite of many efforts spanning over 30 years [16]. The five competing fundamental hypotheses of chirality that have been identified are: 1. The classical hypothesis of macroscopic molecular models (basically van't Hoff description of spontaneous symmetry breaking); 2. The quantum mechanical hypothesis of de facto symmetry breaking with parity conservation, originally from Hund; 3.The super selection-role hypothesis of Pfeiffer and Primas with spontaneous symmetry breaking caused by the influence of the radiation field; 4. The environmental or collision hypothesis of Simonius, Harris, and Stodolsky that induces de facto symmetry breaking in chiral molecules because of interactions with an external medium; 5. The hypothesis of de lege symmetry breaking in chiral molecules because of parity violation [17].

Except for glycine, all of the amino acids isolated from proteins have four different groups attached to the α-carbon atom. In such a case, the α-carbon is named asymmetric or chiral and the two possible configurations for the α-carbon constitute nonsuperimposable mirror image isomers, or enantiomers. Enantiomeric molecules display a special property called chirality and they own the ability to rotate the plane of polarization of linear polarized light. Clockwise rotation of incident light is referred to as dextrorotatory behavior, and counterclockwise rotation is called levorotatory behavior (figure 1.2). The magnitude and direction of the optical rotation depend on the nature of the amino acid side chain. The temperature, the wavelength of the light used in the measurement, the ionization state of the amino acid, and therefore the pH of the solution, can also affect optical rotation behavior [18].

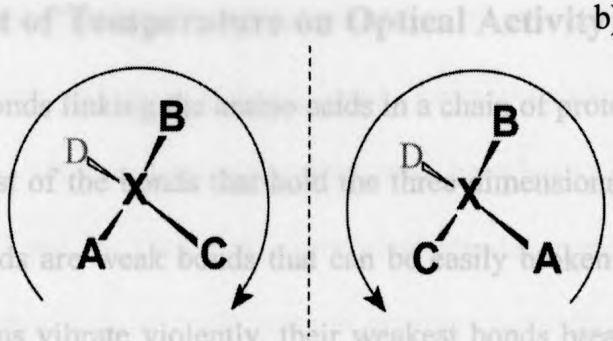

Figure 1.2. *a) dextrorotatory and b) levorotatory behavior of chiral materials (Adopted from [18])*

In general, the optical activity of proteins is due to two factors- the asymmetry of the polypeptide chain and the asymmetry at the α-carbon atoms in amino acid residues. If the asymmetric order of folding of the chain is destroyed, the protein is still optically active because of the rotatory contributions of all the asymmetric α-carbon atoms in the disorganized chain [1]. For example, α-helix can exist in the form of mirror images. A right-handed coil constitutes a mirror image of a left-handed coil. In the case of proteins, a right-handed helix of l-amino acids is a mirror image of a left-handed helix of d-amino acids. Thus, regardless of the optical activity of the component amino acids, a helical structure by itself makes a contribution to the total optical activity of the molecule. The optical rotation of a protein consists of the sum of the rotations of its amino acids and those of its α-helical segments. Accordingly, we can get an indication of the extent of helical structure by determining the difference between the optical rotation of the native protein and that of the amino acid mixture obtained by hydrolyzing the protein. That helix has an optical activity can be demonstrated directly. Of all the amino acids, only glycine lacks a chiral carbon and has no optical rotation. However, polyglycine, a synthetic polypeptide of glycine, forms α-helix and possesses optical activity. The optical rotation of polyglycine results entirely from the asymmetry of the α-helix [19].

1.4. Effect of Temperature on Optical Activity and Protein Structure

The bonds linking the amino acids in a chain of protein are strong covalent bonds. However, most of the bonds that hold the three-dimensional shape of proteins, typically hydrogen bonds are weak bonds that can be easily broken by chemicals or heat. When heated, proteins vibrate violently, their weakest bonds break, and their strings of amino acids begin to unravel [20]. These structural changes because of the temperature effect on the native configurational structures leads to the changes in the specific rotation of proteins [20].

Perlmann [21] investigated the effect of temperature on the optical rotatory properties of pepsin. She observed that at 250 °C the optical rotatory properties of pepsin do not undergo changes if "hydrogen-bond breaking" or "hydrogen-bond strengthening" reagents are added to a pepsin solution. But she showed that the specific rotation $[\alpha]_{546}$ (specific rotation at wavelength of 546 nm) and $[\alpha]_{365}$ (specific rotation at wavelength of 365 nm), respectively, increase slightly if the temperature is raised from 40 to 60 °C [21]. In a study on zein (a class of plant protein), it was found that increasing the temperature to 70 °C in 80 % ethanol-water solution yielded reversible changes in the primary structure (20 % reduction in absolute magnitude of $[\alpha]_\lambda$ at 208 and 222 nm) and tertiary structure (40 % reduction in absolute magnitude of $[\alpha]_\lambda$ at 268 nm) [22].

1.5. Chiroptical Methods

Chiroptical methods are optical methods that can differentiate between two enantiomers. They include polarimetry, optical rotatory dispersion (ORD), and circular dichroism (CD) [31]. Perhaps in no other area of biochemistry have the chiroptical techniques been used for conformational analysis with greater advantage than in the field

of peptides and proteins [1]. The applications of chiroptical methods in the studies of protein structure are described in many review articles [23,24,16]. The important advances in far- ultra violet spectropolarimetry have been reviewed by Harrinton, Joseph, and Segal [25] and by Yang [26]. Several articles have appeared on the optical rotatory dispersion method and its application in organic chemistry [27-29]. Chiroptical methods are based on the interaction of monochromatic polarized light with the valence electron shells of the atoms of a substance. The result of this interaction is the phenomenon of rotatory dispersion. This phenomenon depends on the arrangement of the atoms in the space and on the wavelength of the light which strikes them. Thus a polypeptide chain in helical arrangement yields different effects from those displayed by a disordered chain [1]. Detection is based on the interaction between a chiral center in the analyte and the incident polarized electromagnetic radiation [30].

1.5.1. Polarimetry and Optical Rotatory Dispersion (ORD)

Light is a transverse electromagnetic wave associated with a magnetic, $\vec{H}$, and an electric, $\vec{E}$, field (figure 1.3). For unpolarized light, the electric vector, $\vec{E}$ may oscillate in any direction perpendicular to the direction of propagation, $\vec{x}$. For linearly polarized light, the electric vector oscillates in a single direction [32].

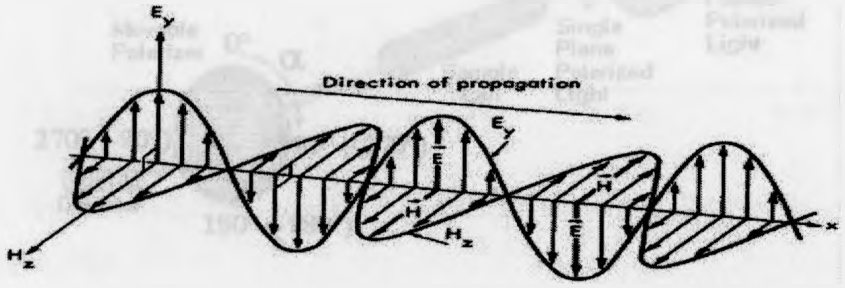

Figure 1.3. *A propagating electromagnetic wave. The sinusoidally oscillating magnetic field, $\vec{H}$, is oriented perpendicular to the sinusoidally oscillating electric field, $\vec{E}$, and both are perpendicularly oriented with respect to the propagation direction , $\vec{x}$. (Adopted from [33]).*

Polarimetry and ORD both are techniques to determine the extent to which a beam of linearly polarized light rotates on transmission through a medium containing a chiral sample [34] (figure 1.4).

The degree of rotation is dependent on the rotatory strength of the chiral center, the concentration of the chirophore, and the path length :

1.5.1) $[\alpha]_\lambda = 100\ \theta / (c\ l)$,

1.5.2) $[m]_\lambda = 10^{-2}\ M\ [\alpha]_\lambda$

where θ, $[\alpha]_\lambda$, and $[m]_\lambda$ are the rotation in degrees, specific rotation and molar rotation at the wavelength λ , respectively. M the molecular weight of the sample; l the optical path length through the solution in decimeters and c is the concentration of the optically active solute in grams per 100 ml. The specific rotation of chiral material, $[\alpha]_\lambda$ is defined as the observed angle of optical rotation, when plane-polarized light is passed through a sample with a path length of 1 decimeter and a sample concentration of 1 gram per 1 millilitre [34].

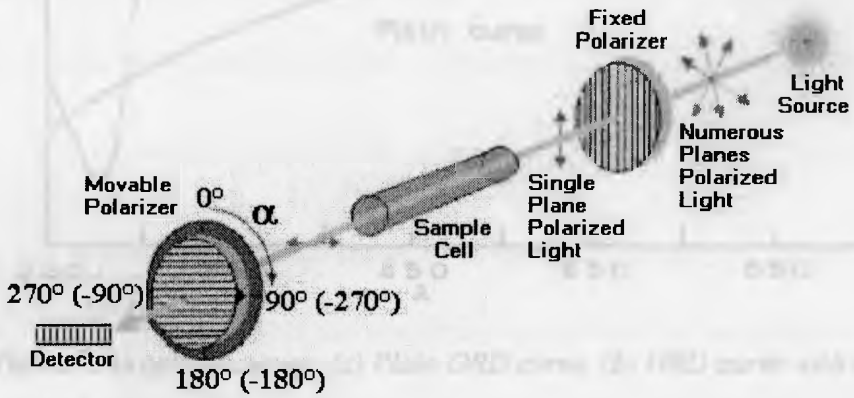

Figure 1.4. *Plane of polarization of a linearly polarized light beam is rotated by an optically active solution (Adopted from [34]*

These two techniques are equivalent for nonabsorbing chiral species and differ only in that ORD yields a spectral response depended on the wavelength, whereas polarimetric measurements usually are restricted to a limited number of preselected wavelengths [30]. In the absence of absorption, the plain ORD spectrum changes monotonically with wavelength. This change can be either positive or negative. For chiral media that absorb the polarized light beam, anomalous rotations in the ORD spectrum are produced if the chiral center and the chromophore are structurally adjacent to each other in an arrangement called a chirophore. This anomalous behavior is referred as the Cotton effect and is limited to the wavelength range of the absorption band, where it is seen superimposed on the monotonically changing plain curve [31] (figure1.5).

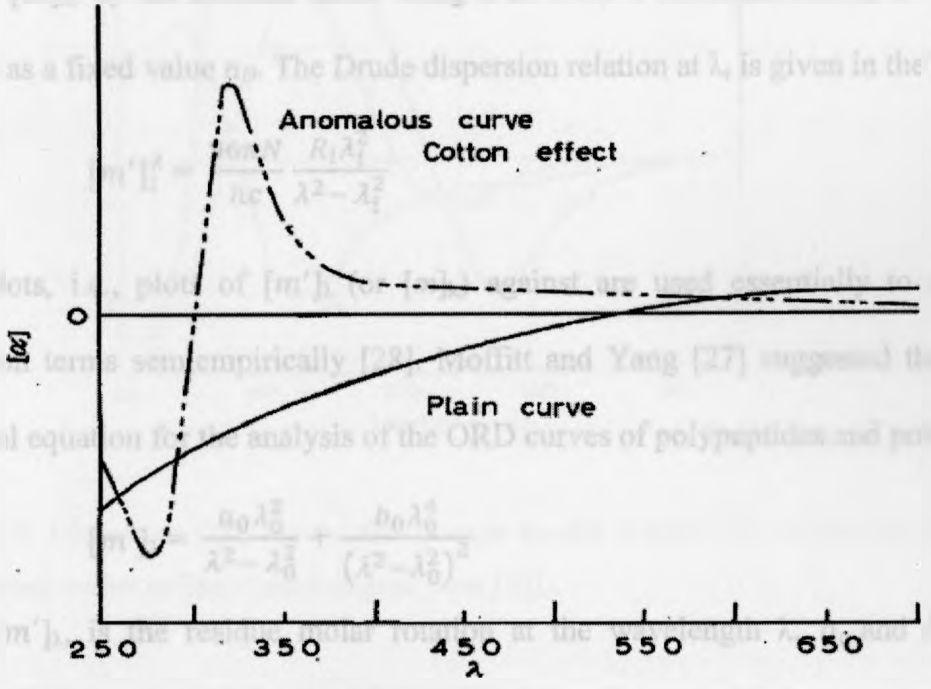

Figure 1.5. *Typical chiroptical curves. (a) Plain ORD curve, (b) ORD curve with a Cotton effect (Adopted from [30])*

These methods have been used in the study of protein structure [1]. The ORD

spectra of poly-L-lysine in the α-helical, antiparallel β-pleated sheet and random coil conformations are illustrated in figure 1.6 [35]. In the case of polypeptides, proteins, and other biopolymers, one often expresses $[m]_\lambda$ in equation 1.5.2 as residue molar rotation, where the mean residue molecular weight (mean monomer weight) M_o, is substituted for M. The mean residue rotation is further corrected for the effect of the polarizability of the medium on the effective field seen by the sample, the Lorentz correction, to yield the reduced mean residue rotation:

1.5.3) $$[m']_\lambda = [m]_\lambda \frac{3}{n_\lambda^2+2}$$

where n_λ is the refractive index of the solvent at wavelength λ. Ideally one should then correct $[m]_\lambda$, by the Lorentz factor using n at every λ of measurement; it is, however, chosen as a fixed value n_D. The Drude dispersion relation at λ_i is given in the form

1.5.4) $$[m']_i^\lambda = \frac{96\pi N}{hc} \frac{R_i \lambda_i^2}{\lambda^2 - \lambda_i^2}$$

ORD plots, i.e., plots of $[m']_\lambda$ (or $[m]_\lambda$) against are used essentially to analyze the dispersion terms semiempirically [28]. Moffitt and Yang [27] suggested the following empirical equation for the analysis of the ORD curves of polypeptides and proteins.

1.5.5) $$[m']_\lambda = \frac{a_0 \lambda_0^2}{\lambda^2 - \lambda_0^2} + \frac{b_0 \lambda_0^4}{(\lambda^2 - \lambda_0^2)^2}$$

where $[m']_\lambda$, is the residue molar rotation at the wavelength λ, a_0 and b_0, are two characteristic constants that reflect the conformational status of the polymer, and λ_0 is an empirical constant usually fixed at 212 nm. Analysis of a large number of polypeptides and proteins has yielded the value of b_0 = 630 as the characteristic value for a completely α-helical polypeptide chain (with λ_o= 212 nm). with randomly coiled segments, b_0 has a

value close to zero. The term a_0 usually does not display such a conformation-dependent constancy, and its value depends on several factors such as the solvent, the nature of the side chains, and the primary structure of the polypeptide or proteins [35].

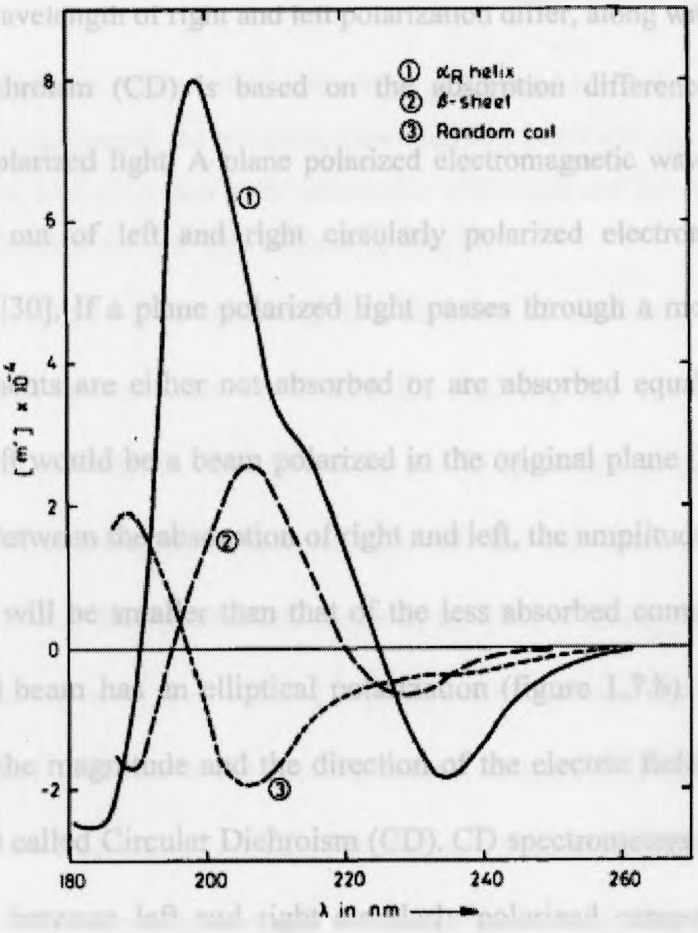

Figure 1.6. *Ultraviolet ORD curves for (1) right-handed α-helix, (2) antiparallel β-sheets, and (3) randomly coiled polypeptides (Adopted from [35]).*

1.5.2. Circular Dichroism (CD) Spectrometry

CD is the most sophisticated of the three chiroptical methods in that the rotation and absorbance measurements are made simultaneously. For circular polarized light, the electric field vector rotates about its propagation direction while retaining constant magnitude

(the electric field forms a helix while propagating). For left circularly polarized light, with propagation towards the observer, the electric vector rotates counter-clockwise, while for right circularly polarized light, the electric vector rotates clockwise. When circularly polarized electromagnetic wave passes through an absorbing optically active medium, the speed and wavelength of right and left polarization differ, along with the extent of absorption. Circular dichroism (CD) is based on the absorption difference between left and right circularly polarized light. A plane polarized electromagnetic wave can be viewed as being constructed out of left and right circularly polarized electromagnetic waves of equal magnitude. [30]. If a plane polarized light passes through a medium in which right and left components are either not absorbed or are absorbed equally, the recombination of right and left would be a beam polarized in the original plane (figure 1.7.a). If there is a difference between the absorption of right and left, the amplitude of the stronger absorbed component will be smaller than that of the less absorbed component, and therefore, the recombined beam has an elliptical polarization (figure 1.7.b). For elliptically polarized light, both the magnitude and the direction of the electric field vary. The occurrence of ellipticity is called Circular Dichroism (CD). CD spectrometers measure the difference in absorbance between left and right circularly polarized components. The difference in absorbance is generally reported in terms of the ellipticity (h) in degrees

1.5.6) $$h = \tan^{-1}(b/a),$$

where, a and b are the minor and major axes of the resulting ellipse, respectively (figure 1.7.b).

a) b)

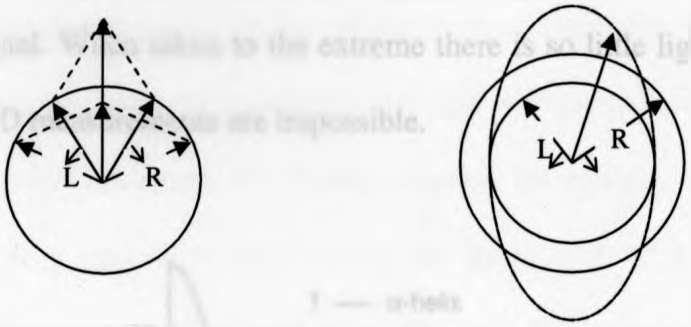

Figure 1.7. a) *When the intensities and phases of the two circularly polarized light beams (R and L) remain the unchanged, the recombination leads to a beam with a polarization that lies in the original plane. b) A difference in the absorption of the right and left circularly polarized beams causes elliptically polarized light.(Adopted from [36])*

When ellipticity is measured as a function of wavelength, a CD spectrum can be obtained. CD spectra have been used for studying the conformation of proteins and polypeptides [37-40]. In the application of CD to analytical problems, the two physical properties of chirality and absorption provide the information necessary for qualitative and quantitative determinations, respectively [30]. Finding correlations within certain spectral features with well-defined peptide conformations has been used for developing computational procedures for conformational analysis [12, 40,41]. By these procedures, estimating the fractions of α-helix, β-strand and β-sheet as well as various types of bends present in a test polypeptide will be possible [38]. Figure 1.8 shows the fingerprint spectra of various proteins secondary structures [39]. Despite of wide use of CD in protein investigations, the limitations of this method should be considered. CD is measured in or near the absorption bands of the molecule of interest, while ORD can be measured far from these bands. Measurement of CD is also complicated by the fact that many solvents used in the biological solutions absorb light in the CD spectral regime. This issue reduces the amount of light available for the measurement and adds nothing to the CD signal. When taken to the extreme there is so little light passing through the

to the CD signal. When taken to the extreme there is so little light passing through the sample that CD measurements are impossible.

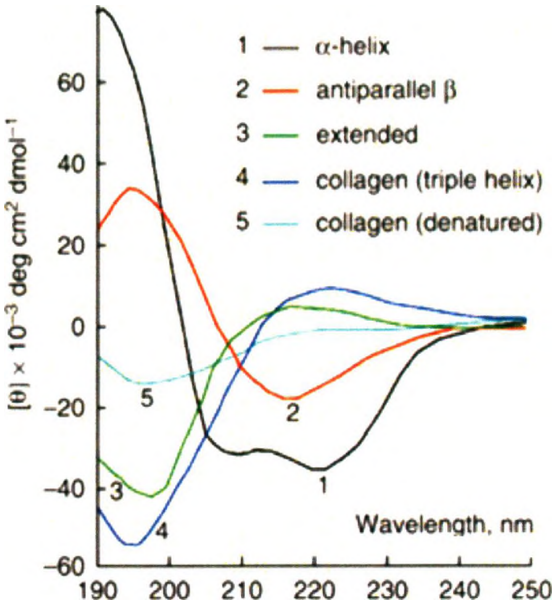

Figure 1.8. *CD spectra of α-helix (black), anti-parallel β-sheet (red), extended (green), native collagen (blue), and denatured collagen (cyan). (Adopted from [39])*

1.6. Purpose of Thesis

The objective of this thesis is to develop a new high sensitivity spectral polarimeter for application in protein and enzyme research, particularly measuring the kinetics of structural changes. The novelty is to implement a hollow optical fiber as the sample cuvette into a polarimeter to enhance the interaction length between the light beam and the sample up to 100 fold [42]. As explained in 1.4 the optical rotation angle θ of a chiral molecule depends on the concentration of the material c, its specific rotation α, which is wavelength (λ) dependent, and the length *l* of the cuvette used. Commercial polarimeters operate with cuvettes in the cm regime. In this thesis, we are able to enhance

length a direct measurement of the optical rotator dispersion $\alpha(\lambda)$ can be taken by scanning the wavelength and measuring the optical rotation angle. A change in the secondary or tertiary structure of proteins changes the optical rotatory dispersion. By taking spectra of a protein solution during the application of a chemical or physical stimuli will enable us to observe the kinetic behavior of this structural change.

There has been a huge amount of efforts to develop novel strategies for structural change investigations based on the optical activity property of proteins.

Christina et al. explored the use of polarized light absorption spectroscopy (linear dichroism (LD)) to study the orientation and binding geometry of a membrane-associated protein hosted in a lipid bilayer of a large (100 nm in diameter) unilamellar lipid vesicle [43]. Tanaka et al. developed a polarization-modulation spectroscopy based on an accurate calibration method that can calibrate CD spectra measured using a conventional photoelastic modulator and perform an accurate analysis of protein secondary structures. [44]. Karno et al. used a direct detection approach via laser-based polarimetry and provided measurements of 19 of the 20 naturally occurring amino acids [45]. All of the mentioned methods implemented a typical cm-sized cuvette sample system.

There are also some attempts to implement an optical fiber in polarimetry. Muhammad at al. used optical fiber polarimeter as a chemical biosensor to show that the presence of a layer of proteins can be sensitively detected via phase change measurements [46]. Heideman et al. did similar investigations in with interaction lengths of the prepared fiber with 5 cm [47]. In another attempt, Wei et al. implemented a liquid-core optical fiber as a cuvette for the detection of different elements and showed an increase in the

sensitivity [48]. However, they built an absorption spectrophotometer setup. Belz carried out similar absorption experiments with a fiber in the UV range [49].

1.7. References

1. Jirgensons, B., *Optical Activity of Proteins and Other Macromolecules.* 1973: Springer-Velberg New York . Heidelberg . Berlin

2. C.A. Floudas,S.R. McAllister, M. Monningmann, R.Rajgaria, *Advances in protein structure prediction and de novo protein design : A review.* Chemical Engineering Science, 2006. **61**: p. 966-988.

3. Branden, C., and J. Tooze, *A non-technical introduction to protein structure.* 1998, Garland Press: New York.

4. Gorga, F.R., *Introduction to Protein Structure.* 1999: Availabe online.

5. *http://en.wikipedia.org/wiki/Protein_structure.*

6. Havel, H.A., *Spectroscopic methods for determining protein structure in solution.* 1996, New York.

7. Baldwin RL, *Is protein folding hierarchic? II. Folding intermediates and transition states.* Trends Biochem Sci, 1999. **24**(2): p. 77-83.

8. Floudas, C.A., *Computational methods in protein structure prediction.* Biotechnology and Bioengineering, 2007. **97**(2).

9. J. L. Klepeis and C. A. FLoudas, *Hybrid global optimization algorithms for protein structure prediction: Alternating hybrids.* Biophysical Journal, 2003. **84**(2): p. 869-882.

10. Beavis RC, *Rapid, sensitive analysis of protein mixtures by mass spectrometry.* Fresenius J Anal Chem, 1992. **343**(25).

11. S.V. Shlyapnikov, V.A. Kulikov and G.I. Yakovlev, *Express analysis of protein amino acid sequences: Primary structure of Penicillium chrysogenum 152A guanyl-specific ribonuclease.* Federation of European Biochemical Societies 1986. **196**(1): p. 29-33.

12. Fasman, G.D., *Circular Dichroism and the Conformational Analysis of Biomolecules* 1996: New York, Plenum Press.

13. Juan Wang, Zhanxia Zhang, Fan Yang, and Xiurong Yang, *Real-time study of genomic DNA structural changes upon interaction with small molecules: Using Dual-Polarization Interferometry.* Anal. Chem, 2009. **81**: p. 4914–4921.

14. Heremans,K., *Review: Protein structure and dynamics at high pressure.* Biochimica et Biophysica Acta, 1998. **1386**: p. 353-370.

15. Gilat, G., *Chiral interactions in protein structures.* Molecular Engineering, 1990. **1**(2): p. 161-178.

16. Chela-Flores, J., *Comments on the origin of chirality in protein amino acids.* Chirality, 1994. **6**: p. 165-168.

17. Quack, M., *How Important is Parity Violation for Molecular and Biomolecular Chirality?* Angewandte Chemie International Edition, 2002. **41**(24): p. 4618-4630.

18. Grisham, G.a., *Molecular components of cells*, in *Biochemistry*, Available online.

19. Stenesh, J., *Biochemistry*. Vol. 1. 1998, New York: Plenum.

20. Cain, *Heat Changes Protein Structure*. Third ed. 2006: Discover Biology.

21. Perlmann, G.E., *Effect of solvents and of temperature on the optical rotatory properties of pepsin.* Biochemistry, 1959. **45**: p. 915-922.

22. Gordon W. Selling and David J. Sessa, *Effect of solvent and temperature on secondary and tertiary structure of Zein by Circular Dichroism.* Cereal Chemistry, 2007. **84**(3): p. 265-270.

23. Urnes Peter and Doty Paul., *The optical rotatory dispersion of right-handed α-helices in sperm whale myoglobin* Proc Natl Acad Sci, 1961. **47**(10): p. 1635–1641.

24. Jirgensons, B., *Optical rotatory dispersion and conformation of various globular proteins.* The Journal of Biological Chemistry, 1963. **238**(8): p. 2716-2722.

25. W F Harrington and D M Segal, *Physical chemical studies on proteins and polypeptides.* Annu. Rev. Biochem, 1966. **35**: p. 599-650.

26. Yang, J.Y., *Effect of molecular aggregation on circular dichroism and optical rotatory dispersion of helical poly-L-glutamic acid in solution.* Biochemical and Biophysical Research Communications, 1967. **26**(1): p. 58-64.

27. William Moffit., A. Moscowitz, W. Klyne, Carl Djerassi, *Structure and the optical rotatory dispersion of saturated ketones.* journal of American Chemistry Society, 1961. **83**(19): p. 4013-4018.

28. Holden-Day, *Optical rotatory dispersion and circulardichroism in organic chemistry.* Angewandte Chemie International Edition, 1965. **78**(7): p. 347-400.

29. Snatzke, G., E d *Optical rotatory dispersion and circular dichroism in organic chemistry.* 1967, London: Heyden.

30. Swallows, N.P., *Analytical applications of polarimetry, optical rotatory dispersion, and circular dichroism.* American Chemical Society, 1989. **61**(2).

31. Gergely, A., *A review of the application of chiroptical methods to analytical chemistry.* Journal of Pharmaceutical & Biomedical Analysis, 1989. **7**(5): p. 523-541.

32. Henry Erying and Dennis Caldwell, *Optical rotatory dispersion and circular dichroism.* Chemical Reviews, 1968. **68**(5): p. 525-540.

33. Hawksford, M.O. (1995) *Electrical Signal Propagation & Cable Theory.*

34. Eliel, E.L., *Stereochemistry* Encyclopedia of Physical Science and Technology, 2004: p. 79-93.

35. Balasubramanian,M., Kumar,C., *Recent Studies of circular dichroism and optical rotatory dispersion of biopolymers.* Applied Spectroscopy reviews, 1976. **11**: p. 223-286.

36. N. Berova and R.W. Woody, *Circular dichroism, principals and applications*. Second ed. 2000: A John Wiley & Sons, Inc., Publication.

37. A. Perczel, and G.D. Fasman *Analysis of the circular dichroism spectrum of proteins using the convex constraint algorithm: A practical guide.* Anal. Biochem, 1992. **203**(1): p. 83-93.

38. Fasman, G.D., *Circular dichroism and the conformational analysis of biomolecules*, N.Y.P. Press, Editor. 1996.

39. Greenfield, N.J., *Using circular dichroism collected as a function of temperature to determine the thermodynamics of protein unfolding and binding interactions.* Nature Protocols, 2006. **1**(6): p. 2527-2535.

40. S. Y. Venyaminov, e.a., *Circular dichroic analysis of denatured proteins: Inclusion of denatured proteins in the reference set.* Anal. Biochem, 1993. **214**(1): p. 17-24.

41. Johnson, W. *Analysis of circular dichroism spectra.* Methods in Enzymology, 1992. **210**: p. 426-447.

42. T. C. Preston, S. Stille, N. D. Jones and S. Mittler, *Simple liquid-core waveguide polarimetry.* Applied Physics Letters 2006. **89**.

43. Christina E., B. Caesar, Per Lincoln, and Bengt Norde´n, *Assigning membrane binding geometry of cytochrome c by polarized light spectroscopy.* Biophysical Journal, 2009. **96**: p. 3399-3411.

44. Masahito Tanaka, Fusae Kaneko, and Kazumichi Nakagawa, *Accurate and quick calibration method for polarization-modulation spectroscopy using an ac-modulated polarizing undulator.* Review of Scientific Instruments, 2008. **79**.

45. Karno N.G and D. R. Bobbitt, *Direct specific rotation measurements of amino acids, dipeptides, and tripeptides by laser-based polarimetry.* Chirality, 1999. **11**(3): p. 187-194.

46. F. A. Muhammad and J. M. Senior, *Polarimetric optical D-fiber sensor for chemical applications.* Microwave and Optical Technology Letters, 1998. **19**(5): p. 318-321.

47. Rene G. Heideman, *Polarimetric optical-fiber sensor for biochemical measurements.* Sensors and Actuators B, 1993. **12**: p. 205-212.

48. Wei Wang, Qushe He, Jufang Wang, Mingzhao Feng, Guanyan Wu, *Spectrophotometry with liquid-core optical fiber in aqueous solution phase in ultraviolet region.* Analytical Chimica Acta, 1998. **375**: p. 261-267.

49. Belz, M., *Simple and sensitive protein detection system using UV LEDs and liquid core waveguides*, in *Proc. of SPIE*, R.A.L. Tuan Vo-Dinh, Gunter Gauglitz, Editor. 2007, Advanced Environmental, Chemical, and Biological Sensing Technologies V.

CHAPTER 2

FUNDAMENTALS AND PROCEDURES

2.1. Introduction

In this chapter, we will begin by first describing the liquid-core fibre cuvette apparatus, which is common in both setup configurations. Then the previous development on liquid-core optical fibers towards the application of a polarimeter (Preston et al.) will be introduced and discussed. This chapter contains the motivation and fundaments of this Master thesis. The fundamental liquid-core optical fiber polarimeter setup, already available, was used here for testing long fibers of up to 10 m. A simple absorption spectroscopy setup operating in the visible regime will be introduced. This absorption spectrometer was employed for the investigation of absorption issues of fibers filled with different solvents. Finally, the concept of the new high sensitivity spectral fiber polarimeter with all components and their function will be presented.

2.2. Liquid-Core Fiber Cuvette

The cuvette holding the fibers was altered to allow for a quicker fiber exchange. By using a ferrule fitting (C360NFFS, VICI Valco Instruments Co. Inc) implemented in the existing teflon cells, the fiber has been fixed in the cuvette by using only little amounts of silicon glue for sealing. The standard glass cuvette used in polarimetry setups is usually 1-10 cm in length and the sensitivity is at the ppm level [1,2].

The optics of liquid-core fibers is not different from those of conventional optical fibers. It consists of a high refractive index core, cladded by a lower refractive index material that allows the light to propagate through the fiber (figure 2.1.a) by the well-known phenomenon of total internal reflection. Further, because of the cylindrical symmetry in the fiber structure, this ray will suffer total internal reflection at the lower

interface also and therefore will get guided through the core by repeated total internal reflections. Even for a bent fiber, light guidance can take place through multiple total internal reflections (figure 2.1.b) [3]. However, there is a minimum bending radius. If the bending radius is below this minimum, the condition of total internal reflection is not satisfied anymore and light leaks out of the fiber.

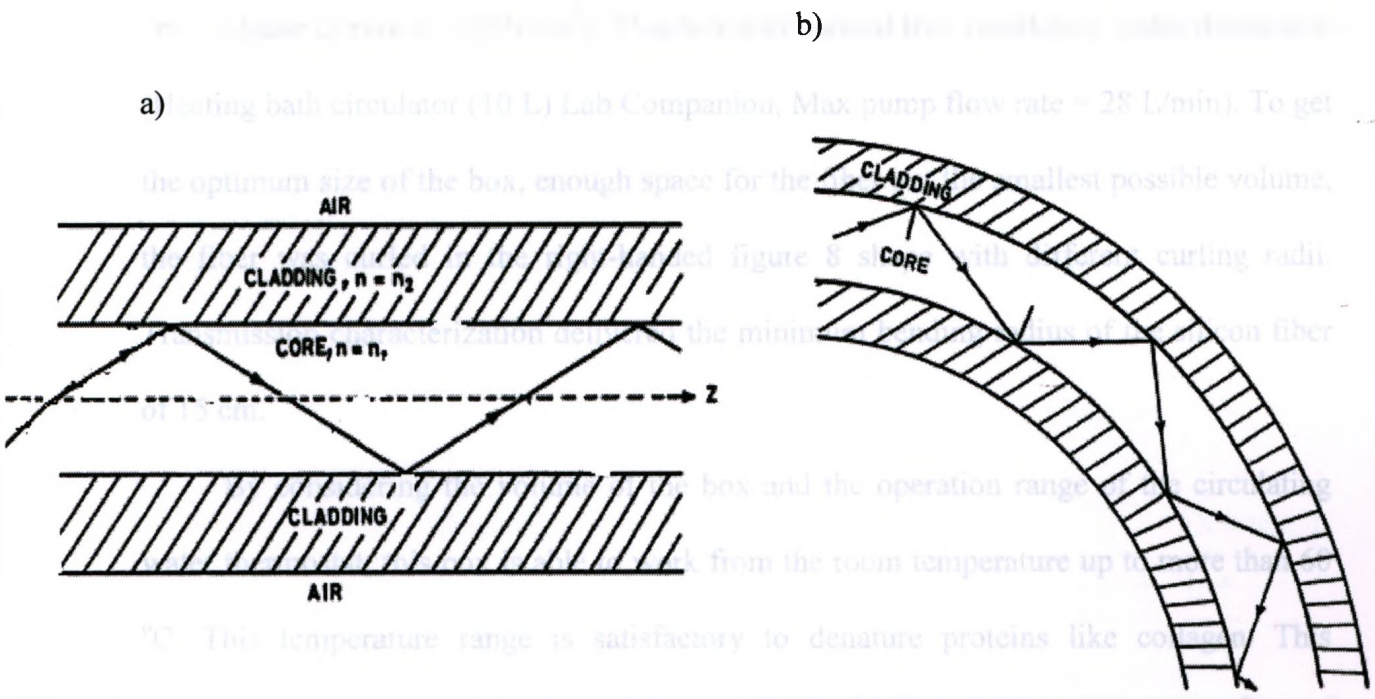

Figure 2.1. *a) A cross section of a hollow core fiber which makes up the solid portion of our liquid-core fiber. When the liquid has a greater index of refraction than the fused silica, total internal reflection occurs ($n_1 > n_2$). b) Rays propagating through a bent fiber (Adopted from[3]).*

In our application, a solvent containing the analyte of interest serves the same function as the high refractive index core of a standard optical fiber. The cladding is a low transmission-loss hollow fiber. Using a fiber as the cuvette, the length of the cuvette can be extended up to 5 m (or 10 m). The advantage of such a fiber is the scalability of path length. It allows for large sensitivity enhancements (results shown in table 2.1) with little or no increase to instrument size or cost [4]. Furthermore, by their very design, these

waveguides are readily incorporated into rapid screening systems [5].

In order to remove the effect of temperature fluctuations on the optical rotatory dispersion of e.g. proteins, that were mentioned in chapter 1, and to conduct denaturing studies triggered by elevated temperatures, the hollow optical fiber cuvette containing the sample solutions was placed inside a home-build temperature stabilized box (35 x 40 x 50 cm, Volume of box = 36000 cm^3). This box was hooked to a circulating water thermostat (Heating bath circulator (10 L) Lab Companion, Max pump flow rate = 28 L/min). To get the optimum size of the box, enough space for the fiber but the smallest possible volume, the fiber was curled in the right-handed figure 8 shape with different curling radii. Transmission characterization delivered the minimum bending radius of the silicon fiber of 15 cm.

By considering the volume of the box and the operation range of the circulating water thermostat, this box is able to work from the room temperature up to more than 60 ^{o}C. This temperature range is satisfactory to denature proteins like collagen. This thermostat makes possible to heat up the sample in the fiber and investigate the effect of temperature on the denaturation process of proteins. In the future, an additional cooling system in the thermostat will enable exploration of temperature cycling.

2.3. Simple Liquid-Core Fiber Polarimeter

In the simple liquid-core fiber polarimeter light from a continuous wave linearly polarized He-Ne laser at a wavelength, λ = 632.8 nm (Research Electro-Optics, 12.0 mW) was coupled into the liquid-core fiber with a microscope objective (10 x, numerical aperture = 0.25, f = 16.5 mm, Newport). The liquid-core fiber consists of fused silica tubing with a 150 μm inner diameter and a 360 μm outer diameter (TSP150375,

Polymicro technologies, Phoenix, Arizona) or teflon AF fiber tubing with a 50 μm inner diameter and a 360 μm outer diameter (2400 Tubing, Random Technologies, San Francisco, California) as depicted in figure 2.2. A cuvette assembly had been designed to hold the fiber and allow injecting liquid. Pumping is required during the filling and emptying process. Typically, first the front cell is filled with the solution by using a syringe. Then the liquid is drawn from the cell into the fiber via a peristaltic pump (EV 500, Autoclude, 60 ml/min). Before launching the laser beam into the fiber it passes through a polarizer to set the polarization direction of the coupled light beam. The emerging polarization was measured by using the beam splitter arrangement (figure 2.2).

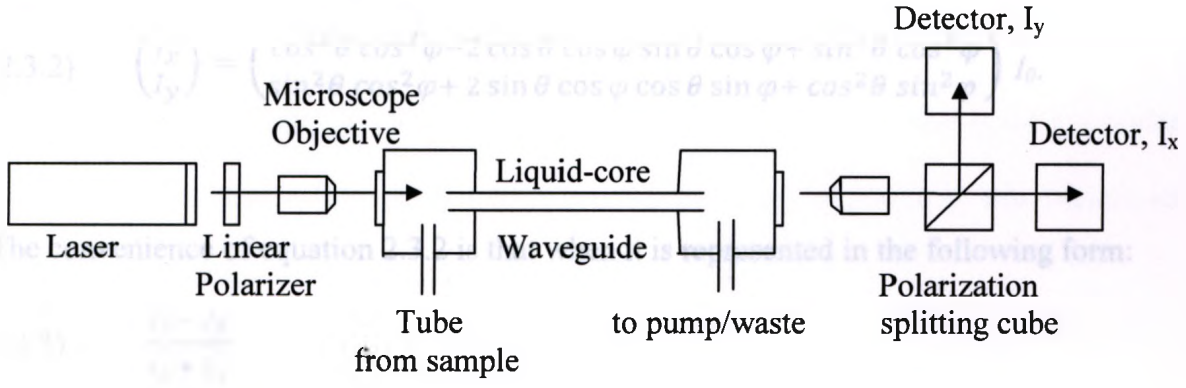

Figure 2.2. *Scheme of the laser liquid-core polarimeter*

In principle, two different detection setups can be applied. When no chiral material is present in the fiber and the fiber shows no Eigen-rotation, only the polarization direction which is launched into the fiber should lead to a detectable intensity. The intensity of the perpendicular polarization direction should be zero. When optical turning occurs due to the presence of a chiral material in the liquid filled hollow fiber both components should show an intensity as long as the turning angle does not happen to be

180 or 360 °[4] .

2.3.1. Theoretical Background

To understand how this is accomplished, first consider the propagation of light in figure 2.2 by using the following Jones calculus representation [6]

2.3.1) $$\begin{pmatrix} E_x \\ E_y \end{pmatrix} = \begin{pmatrix} \cos\theta & -\sin\theta \\ \sin\theta & \cos\theta \end{pmatrix} \begin{pmatrix} \cos\varphi \\ \sin\varphi \end{pmatrix} E_0,$$

where θ is the angle of rotation that results from optical activity present in the core, φ is the angle of the linear polarizer, and E_0 is the time dependent amplitude of the field emerging from that polarizer. Since two detectors measure the intensity, equation 2.3.1 must be multiplied by its complex conjugate to be useful. This yields an equation that relates rotation to what is physically measured,

2.3.2) $$\begin{pmatrix} I_x \\ I_y \end{pmatrix} = \begin{pmatrix} cos^2\theta\, cos^2\varphi - 2\cos\theta\cos\varphi\sin\theta\cos\varphi + sin^2\theta\, cos^2\varphi \\ sin^2\theta\, cos^2\varphi + 2\sin\theta\cos\varphi\cos\theta\sin\varphi + cos^2\theta\, sin^2\varphi \end{pmatrix} I_0.$$

The convenience of equation 2.3.2 is that when it is represented in the following form:

2.3.3) $$\frac{I_x - I_y}{I_x + I_y},$$

simplification allows for rotation to be solved easily as a function of the two measured intensities and the entrance angle φ;

2.3.4) $$\cos(2\theta + 2\varphi) = \frac{I_x - I_y}{I_x + I_y}.$$

Furthermore, the denominator on the right side of equation 2.3.4 normalizes for any intensity fluctuations from the light source.

In order to explore how the optical activity of a dissolved material in the liquid

effects the rotation of polarized light in the liquid-core fiber, several chiral species with different right and left handed optical activities were studied by Preston et al. with two visible wavelengths at λ = 543.5 and 632.8 nm: (R)-(+)-limonene, (S)-(-)-limonene, (S)-(+)-carvone, (R)-(-)-carvone, (1R,5R)-(+)-α-pinene, and (1S,5S)-(-)-α-pinene. Their specific optical rotation, α, was determined according to equation 2.3.5 [4].

2.3.5) $$[\alpha]_\lambda = \frac{\theta}{lc},$$

where θ is the observed rotation angle in degrees, l is the path length of the light beam in dm, and c is the concentration in g/mL. However a more convenient form of equation 2.3.5 is :

2.3.6) $$[\alpha]_\lambda = \frac{10^7\theta}{l' c' MW}$$

where l' is the path length in cm, c' is the concentration in mM, and MW is the molecular weight in g/mol. For reference, a conventional polarimetry experiment was performed using the neat chemicals in 1 cm path length UV/Vis cells.

2.3.2. Test Results of the Simple Fiber Polarimeter

The results for running the chiral solutions through a linear, 26.3 cm long fiber in Thomas work are shown in (table 2.1). "These investigations show that the path length term in (equation 2.3.5) can simply be replaced by fiber length when calculating the optical constants. The equivalence of path length to fiber length, highlights the potential for using a liquid-core waveguide in polarimetry: as the length of the capillary is increased, sensitivity should increase proportionally. Furthermore, because light propagates through total internal reflection, there should be little variation in the intensity of the transmitted beam. In addition, the small diameter of the capillary means that the

volume of sample required to fill the fiber will always be very small compared to conventional cuvettes. For a fiber length of 26.3 cm, the volume of the core is 4.65 μl; for 220.8 cm, it is 38.9 μl. Using a peristaltic pump (EV 500, Autoclude, 60 ml/min), the filling times for these two fibers were less than a second and around 30 s, respectively" [4].

	Specific rotation [α] (10^{-1} cm^2 g^{-1})			LOD (mM)	
	1 cm cell	26.3 cm fiber	220.8 cm fiber	26.3 cm fiber	220.8 cm fiber
λ=543.5 nm					
(*R*)-(+)-limonene	147±1	148±3	145.0±2.4	3	0.3
(*S*)-(−)-limonene	−129±1	−122±5	−130.4±1.3	3	0.3
(*R*)-(−)-carvone	−75±1	−65±3	−65.9±1.5	5	0.6
(*S*)-(+)-carvone	76±1	74±5	66.5±1.4	5	0.6
(1*R*,5*R*)-(+)-α-pinene	59±1	66±3	61.9±0.7	6	0.7
(1*S*,5*S*)-(−)-α-pinene	−58±1	−57±2	−59.9±0.7	7	0.8
λ=632.8 nm					
(*R*)-(+)-limonene	104±1	105±2	103.8±1.0	5	0.7
(*S*)-(−)-limonene	−92±1	−100±2	−93.2±0.5	5	0.8
(*R*)-(−)-carvone	−52±1	−51±2	−44.8±0.5	9	1.4
(*S*-(+))-carvone	53±1	50±3	46.1±0.3	9	1.4
(1*R*,5*R*)-(+)-α-pinene	44±1	41±2	43.1±0.3	13	1.6
(1*S*,5*S*)-(−)-α-pinene	−41±1	−46±4	−42.8±0.1	11	1.6

Table 2.1. *Specific rotations and limits of detection (LOD) for chiral species at the wavelengths of 543 and 632.8 nm and fiber lengths of 26.3 and 220.8 cm (Curled in a RAF8 configuration with two loops of equal radii [4].*

However, extending the fiber to 2, and later in this thesis to 5 and 10 m length, will require curling of the fiber for space reasons. It is well known that curling introduces a birefringence in the fiber in the form of perpendicularly polarized "fast" and "slow" light rays [7]. This birefringence introduces a turning of the polarization direction even without any optically active material in it. This effect can be seen easily when the fiber is curled into a double loop while the angle of polarized light entering the fiber is varying

and the output polarization is being measured (figure 2.3).

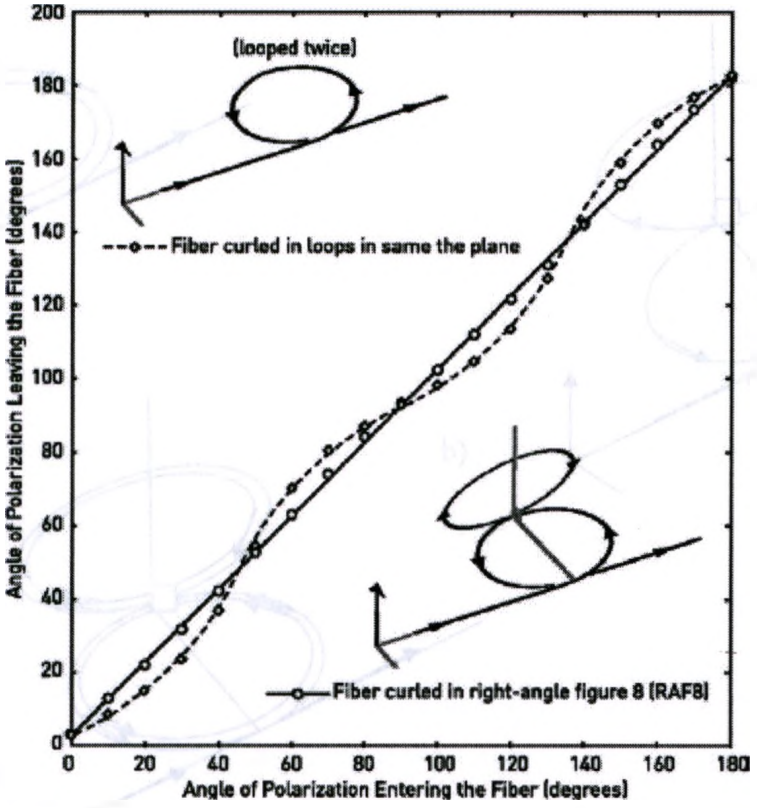

Figure 2.3. *Angle of polarization after passing through a fiber vs the angle of polarization entering a fiber for λ=632.8 nm using a fiber length of 239.7 cm filled with toluene. The fiber was curled into either a double loop or a RAF8 configuration. The angle of 0° is defined as being perpendicular to the plane of the first loop. The radii of all loops are equal (17 cm)[4].*

"These periodic deviations will obscure the true rotation of polarized light by any optically active species present in the fiber core and a fiber curled in this manner would be difficult to use in any practical application without extensive data analysis and calibration. However, by curling the fiber into two loops at right angles to each other and creating a right-angle figure 8 (RAF8) configuration (figure 2.4.b), these deviations will be eliminated as the fast and slow planes will effectively cancel each other over the total distance of the two loops"[2]. For the purpose of characterizing the long fibers, first this curling configuration has been employed for a 2 m fiber by Preston et al.

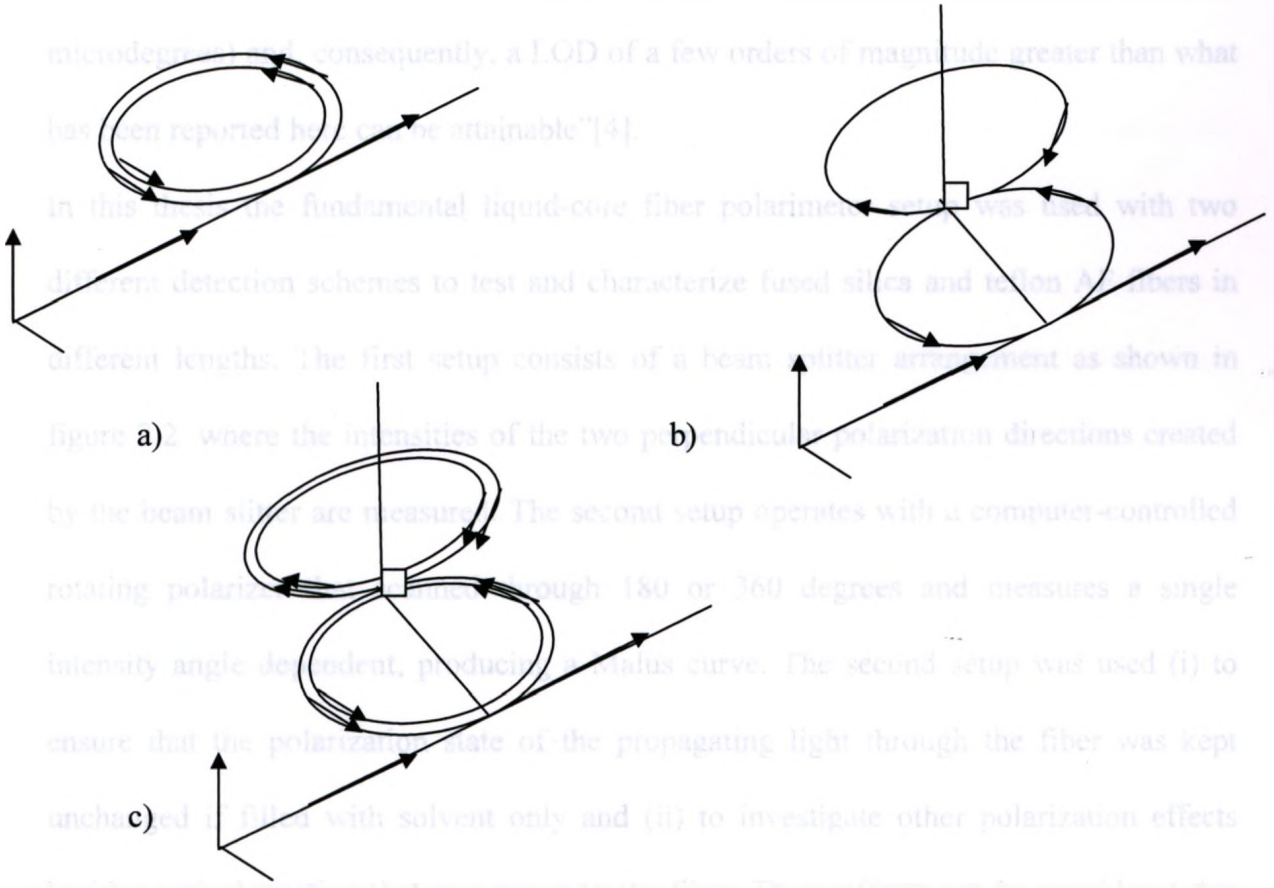

Figure 2.4. *a) Fiber curled into a double loop in the same plane, b) 2m fiber curled into two loops in RAF8 figuration, c) 5m fiber curled in RAF figuration. It shows how to curl the long fibers into more than two loops.*

"With this simple experimental setup changes as small as 90 mdeg (λ = 632.8 nm) and 70 mdeg (λ = 543.5 nm) can be observed. This resolution, however, should not be used as a figure of merit when attempting a comparison to other polarimeters. Only a limit of detection (LOD) that takes into account the additional factors of the optical constant of the sample, the wavelength of light, and the path length of the polarimeter should be used for this type of evaluation. Clearly, path length is the most important advantage of this polarimeter which motivated us to build the new spectral polarimeter. Using new

techniques in the spectral polarimeter setup not employed in this setup, resolutions comparable to those of commercially available instruments (typically on the order of microdegrees) and, consequently, a LOD of a few orders of magnitude greater than what has been reported here can be attainable"[4].

In this thesis the fundamental liquid-core fiber polarimeter setup was used with two different detection schemes to test and characterize fused silica and teflon AF fibers in different lengths. The first setup consists of a beam splitter arrangement as shown in figure 2.2, where the intensities of the two perpendicular polarization directions created by the beam slitter are measured. The second setup operates with a computer-controlled rotating polarizer that scanned through 180 or 360 degrees and measures a single intensity angle dependent, producing a Malus curve. The second setup was used (i) to ensure that the polarization state of the propagating light through the fiber was kept unchanged if filled with solvent only and (ii) to investigate other polarization effects besides optical rotation that may occur in the fiber. These effects can be considered due to polarization mode dispersion (PMD) and polarization-dependent loss (PDL) [8] . However, once the fiber had been characterized, the beam splitter arrangement was used. In this thesis the fiber lengths was extended to 5 and 10 m fibers with multiple curls as shown in figure 2.4.c.

2.4. Investigation of Solvent Effect

The selection of a suitable solvent is influenced by the material under investigation and its solubility in a solvent, by the refractive index of the solvent and by the absorption features of the solvent in the wavelength regime focused on [5]. Since the measurements are supposed to be carried out in the visible, the absorption spectra of

liquid-core fibers filled with various solvents have been investigated in the visible. These experiments were carried out by launching photons from a white light source (Halogen Light Source, HL-2000, Mikropack) via a microscope objective (10 x, numerical aperture = 0.25, f = 16.5 mm, Newport) into the fiber and measuring the transmission spectra with a spectrometer (HR-2000, Ocean Optics. Inc). The following solvents were analysed spectroscopically from 400 nm to 800 nm: water, ethanol, toluene, benzene, isopropanol, ether, acetone and methanol. The spectra were taken at different lengths of fused silica and teflon AF hollow optical fibers.

2.5. Spectral Fiber Polarimeter Design

The laser liquid-core fiber polarimeter technology which operated with a single line laser was expanded into spectral polarimetry to take advantage of the optical rotatory dispersion of chiral molecules. A new spectral polarimeter system has been built by implementing the components already available in the lab and new components (figure 2.5). In this section, this new spectral polarimeter design is explained in 2 parts: the light source and the detection system.

2.5.1. Light Source Introduction to the Fiber

A spectral lamp (150 W Xenon Arc Lamp, Newport), with an emission from 360-2000 nm was coupled via a beam condensing assembly to a grating monochromator (9055- 1/4M Computer controlled, Sciencetech Inc.) depicting a wavelength resolution of 0.5 nm in the output between 400 and 700 nm. The monochromator is controlled by a computer via a serial port. The output port of the monochromator carries a slit which can be varied in width from 10 μm to 5 μm and in height manually. A copper wheel, is placed between the lamp housing and the monochromator's entrance port for noise reduction.

The light exiting the spectrometer is collimated by a lens (PCX F/3, diameter = 25.4 mm, focal length = 75.6 mm) which is placed in approximately 75 mm from the monochromator output slit. The beam then passes a linear polarizer oriented at 75 degree. The reason of this angle choice will be discussed in chapter 3. The polarized light is focused into the liquid-core fiber with a microscope objective (10 x, numerical aperture= 0.25, f= 16.5 mm, Newport). The aim is to launch as many photons as possible in a given wavelength segment, $\Delta\lambda$, into the fiber.

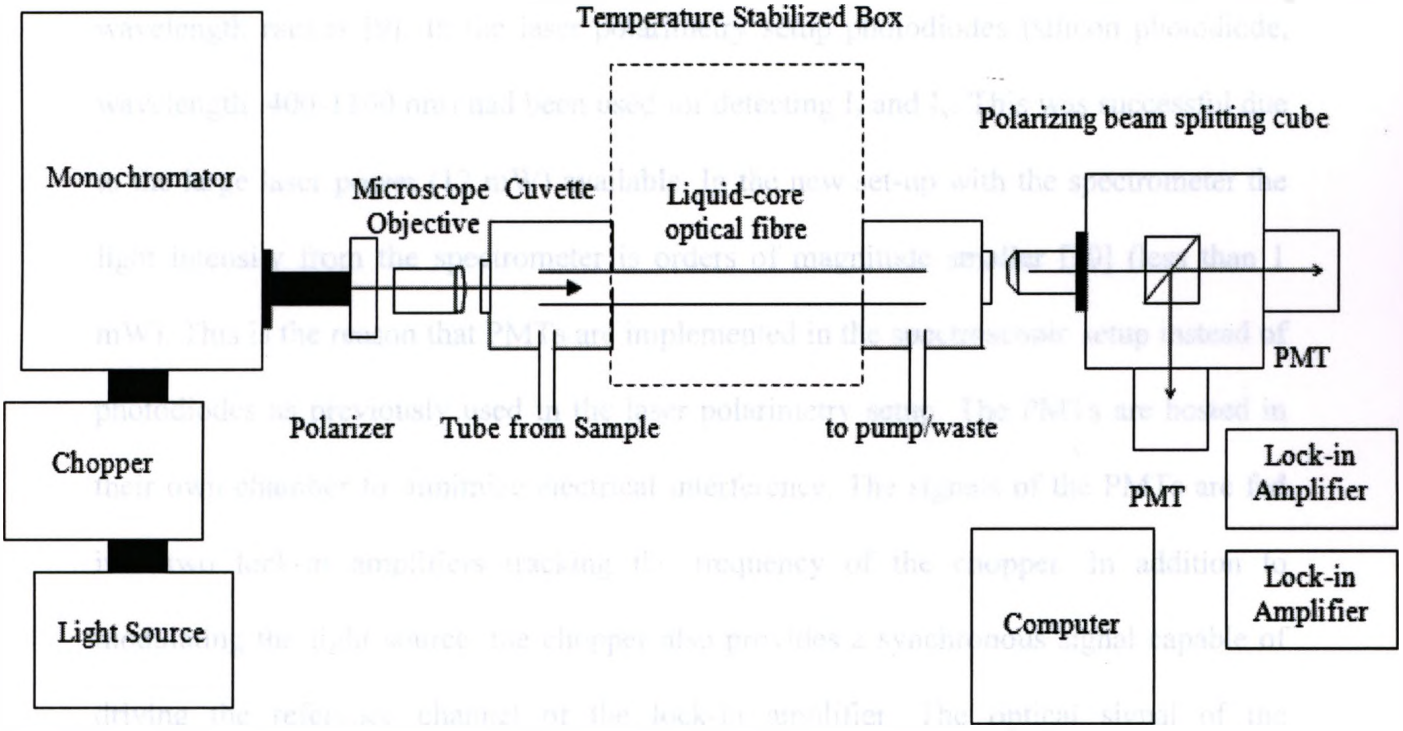

Figure 2.5. *A scheme of Spectral Fiber Polarimeter*

2.5.2. Detection System

The emerging light at the end of the liquid-core fiber cuvette is received by a microscope objective (10 x, numerical aperture= 0.25, f= 16.5 mm, Newport) and guided into a chamber hosting a polarizing beam splitting cube (PBS051, wavelength range:

420-680 nm, Thorlabs). This beam splitter divides the light into two beams propagating with perpendicular polarization and direction towards two photomultiplier tubes (Multialkaline High sensitivity PMT, Hamamatsu) as shown in figure 2.5. Photomultiplier tubes (PMT) are highly sensitive photo-detectors that convert the incoming photons into an electric signal, voltage or current, which can be recorded or measured using standard electronic devices. It consists of a photo-cathode and an electron multiplication system. The photo-cathode converts photons to electrons and the multiplication system amplifies the electric signal. The main application area of the photomultipliers is detection of low light intensities in visible and ultraviolet (UV) wavelength ranges [9]. In the laser polarimetry setup photodiodes (silicon photodiode, wavelength: 400-1100 nm) had been used for detecting I_x and I_y. This was successful due to the large laser power (12 mW) available. In the new set-up with the spectrometer the light intensity from the spectrometer is orders of magnitude smaller [10] (less than 1 mW). This is the reason that PMTs are implemented in the spectroscopic setup instead of photodiodes as previously used in the laser polarimetry setup. The PMTs are hosted in their own chamber to minimize electrical interference. The signals of the PMTs are fed into two lock-in amplifiers tracking the frequency of the chopper. In addition to modulating the light source, the chopper also provides a synchronous signal capable of driving the reference channel of the lock-in amplifier. The optical signal of the experiment falling on the PMTs generates an electrical current which can be measured by the lock-in amplifier. Any discrete frequencies or noise voltage not equal to the reference frequency are rejected by the lock-in amplifier. This allows the operation of the polarimeter under the artificial light from a bulb. The analog output signals are fed into a

data acquisition system digitizing the data and store them in a computer. A computer with a LabView program controls the monochromator and plots the two PMT signals according to equation 2.3.3, while scanning the spectrometer. Recalculating with equation 2.3.4 yields the optical rotator dispersion curve.

2.6 References

1. Wang Wei, W.G., Xu Zheng, Liao Yuanmin,He Qushe, Wang Jufang and Feng Mingzhao, *Study on UV/VIS liquid-core optical fiber long lightpath absorption system for spectrophotometer*, in *SPIE*. 2005.

2. Wang Wei, Wang Tao, Fen Minzhao, Liao Yuanmin, and Ran Gouxia, *Absorbance study of liquid-core optical fibers in spectrophotometry.* Anal. Chem., 1992. **64**: p. 22-25.

3. Thyagarajan, A., *An introduction to fiber optics*. 1998, cambridge: Press Syndicate of the University of Cambridge.

4. Thomas C. Preston, Nathan.D.Jones., Sven Stille and Silvia Mittler, *Simple liquid-core waveguide polarimetry.* Applied Physics Letters, 2006. **89**.

5. Belz, M. *Simple and sensitve detection system using UV LEDs and liquid core waveguides*. in *SPIE*. 2007.

6. Pedrotti,L. and Pedrotti, F., *Introduction to optics*. 1987, Prentice Hall, Englewood Cliffs, NJ, P:353.

7. Thyagarajan, A., *Introduction to Fiber Optics*. 1998, Cambridge: cambridge University Press.

8. Morkel, P.R., Haxell, I.A, Taylor, M.G, Keys, R.;, *Polarisation effects in long-haul optically amplified lightwave systems*, in *IEEE International Conference* 1995: Seattle, WA , USA p. 616-620.

9. Tkachenko, N.V., *Optical Spectroscopy (Methods and Instrumentations)*. 2006: Elsevier.

10. Newport. *Monochromator Throughput*. 2011 [cited].

CHAPTER 3

CHARACTERIZATION AND EXPERIMENTAL SETUP RESULTS AND CONCLUSION

3.1. Introduction

In this chapter, first results will be discussed obtained with the liquid-core optical fiber polarimeter for fibers up to 10 m. To gain the best efficiency from the spectral polarimeter setup and optimize the function of it, each part was characterized and optimized individually. In order to prove the spectral fiber polarimeter works properly and shows an improvement due to the enhanced sample interaction length, the polarimeter was tested with a known material and fibers with different length. The optical rotatory dispersion of the chiral materials was investigated. Those results and discussion on the effect of fiber length on the sensitivity of the spectral polarimeter will be presented.

3.2. Characterization of Fibers

The liquid-core optical fiber polarimeter setup (refer to chapter 2) was applied to characterize the fibers in different length. In most experiments, fused silica fibers were implemented as the liquid core waveguide capillary cuvette. The refractive index of the fused silica mantle is 1.45 at 632.8 nm. Since many biological sample solutions are aqueous with a refractive index slightly above 1.33, teflon AF hollow optical fibers with a mantle refractive index of 1.29 were introduced, otherwise, total internal reflection is impossible. Due to their refractive index, they can be applied as liquid-core waveguide for water based samples.

First, the fiber response was determined with toluene filled silica fibers at 28 and 226.4 cm length at the wavelength of 632.8 nm with the simple laser polarimeter. For various well known chiral materials the specific rotation was measured. For these experiments the long fiber was curled in the RAF figuration. Table 3.1 presents the results obtained

using equation 2.4. All these chemicals have been purchased from Sigma-Aldrich and prepared in toluene with a concentration of 5 mM. The volume of solution for filling the capillary for a fiber length of 28 and 226.4cm was 4.96 and 40 μL, respectively. All loops were curled in an equal radius of 15 cm.

Chiral Materials	Specific Rotation [α] (10^{-1} cm^2 g^{-1})	
	28 cm fiber	226.4 cm fiber
R-(+)-Limonene	106±2	105.8±0.9
S-(-)-Limonene	-101±4	-95.4±0.7
S-(+)-Carvone	52±2	47.2±0.6
R-(-)-Carvone	-51±3	-43.7±0.8
(1R,5R)-(+)-Pinene	42±2	44.3±0.9
(1S,5S)-(-)-Pinene	-47±2	-45±0.7

Table 3.1. *Specific rotations for right and left-handed chiral materials at the wavelength of 632.8 nm and fiber length of 28 and 226.4 cm. All measurements were carried out at 25 °C.*

The obtained results shown in table 3.1 are generally the same as results seen in table 2.1 in experiments published by Thomas et.al. By increasing the fiber length from 28 cm to 226.4 cm, eightfold gain over the 28 cm fiber was resulted. Also with this simple setup, changes as small as 85 mdeg were measured. The sensitivity was, again, found to be proportional to the fiber length.

In the next step, the silica fiber was extended to 427 cm. In order to characterize this length of fiber, it was filled with toluene and curled in two different ways: 1) four loops aligned in the same plane, and 2) RAF figuration like shown in chapter2 (figure 2.4.c).

Figure 3.1. shows the fiber characterization plot "angle of polarization entering the fiber" versus "angle of polarization leaving the fiber" which depicts the influence of the fiber on the polarization state of the propagating light. It can be clearly seen, that the RAF curling is also successful in the 5 m case to remove the polarization influences from the fiber. The silica fiber can be successfully applied in the polarimeter at this length. The specific rotation of the above mentioned chiral species were tested with this 5 m fiber at the wavelength of 632.8 nm and are presented in Table 3.2.

The errors in the calculated specific rotation data for the 5 m fiber, shows smaller numbers in compared with the 2m one and it resulted in approximately double gain over the 2 m fiber. It confirmed that the interaction length increases by extending the fiber length and leads to more sensitive measurements for polarimetry setup. We tried to implement an 862 cm fiber (curled in 8 loops), but it couldn't be aligned properly as a free space construct. A proper apparatus needs to be constructed here to mount the very long fibers in a stable, alignable manner.

Chiral Chemicals	Specific Rotation [α] (10^{-1} cm^2 g^{-1})
R-(+)-Limonene	105.1±0.3
S-(-)-Limonene	-94.3±0.1
S-(+)-Carvone	47.1±0.4
R-(-)-Carvone	-43.2±0.4
(1R,5R)-(+)-Pinene	42.4±0.2
(1S,5S)-(-)-Pinene	-44.8±0.1

Table 3.2. *Specific rotations for right and left-handed chiral material at the wavelength of 632.8*

nm and a fiber length 427cm. Measurements were conducted at 25 °C.

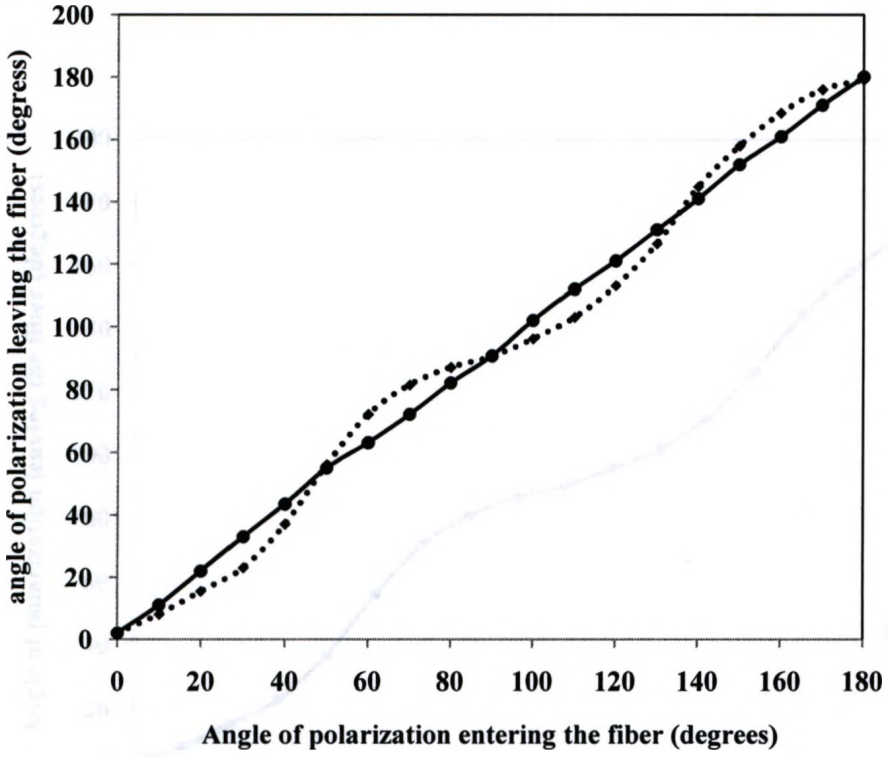

Figure 3.1. *Angle of polarization after passing through a fiber with 427 cm length filled with pure toluene at 632.8 nm. The dashed line shows data for the fiber curled in 4 loops in the same plane and the continuous, straight line shows the data from the fiber curled in RAF 8 figure.*

To explore the applicability of the teflon AF hollow optical fibers in long lengths, a characterization study has been carried out. A 195 cm teflon fiber filled with milli-Q water was curled in two loops laying in the same plane and the polarization changes were recorded (figure 3.2). The result showed the same phenomenon which has been observed in silica optical fibers, however with more pronounced deviations. In order to remove these deviations, the right angle figuration (RAF8) was tried. But because of the soft structure of the teflon fiber, it was completely impossible to fabricate a free-standing RAF figuration. We therefore, conclude that for the longer fibers it is necessary to implement a fiber mount which holds and stabilizes the fiber curling and allows to align

implement a fiber mount which holds and stabilizes the fiber curling and allows to align properly.

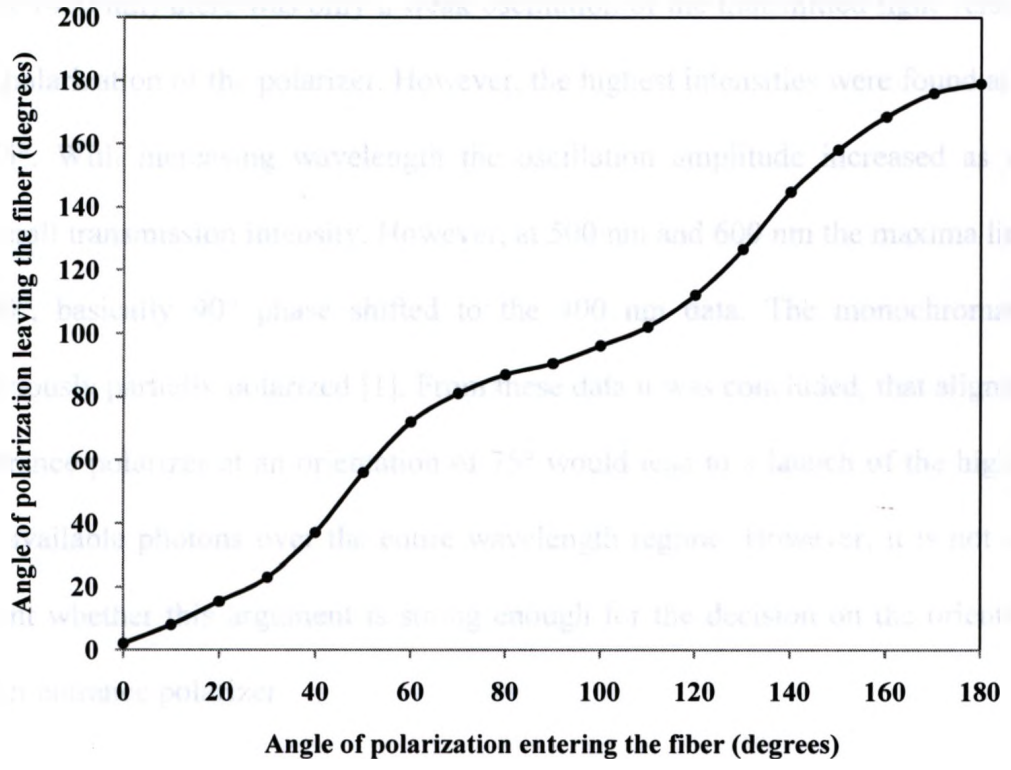

Figure 3.2. *Angle of polarization after passing through a teflon AF hollow optical fiber with 195 cm length at 632.8 nm. The fiber is curled in two loops in a same plane at a radius of 15.2 cm.*

3.3. Investigation of the Polarization State of the Light Leaving the Monochromator

In order to use the monochromator as a light source with the highest possible transmission, the highest possible amount of available photons for launching into the fiber by adjusting the entrance polarizer accordingly, the polarization state of the light leaving the spectrometer was investigated at three different wavelengths covering the spectral regime of interest: 400, 500 and 600 nm. These experiments were carried out by

computer controlled. The light intensity behind the linear polarizer was measured by using a photodiode as a detector. The intensity versus polarization angle results are shown in figure 3.3. The three different wavelength delivered different responses. In the blue (400 nm) there was only a weak oscillation of the transmitted light versus the angle of polarization of the polarizer. However, the highest intensities were found at 0/360° and 175°. With increasing wavelength the oscillation amplitude increased as well as the overall transmission intensity. However, at 500 nm and 600 nm the maxima lie at 75° and 260°, basically 90° phase shifted to the 400 nm data. The monochromator light is obviously partially polarized [1]. From these data it was concluded, that aligning the fiber entrance polarizer at an orientation of 75° would lead to a launch of the highest number of available photons over the entire wavelength regime. However, it is not clear at this point whether this argument is strong enough for the decision on the orientation of the fiber entrance polarizer.

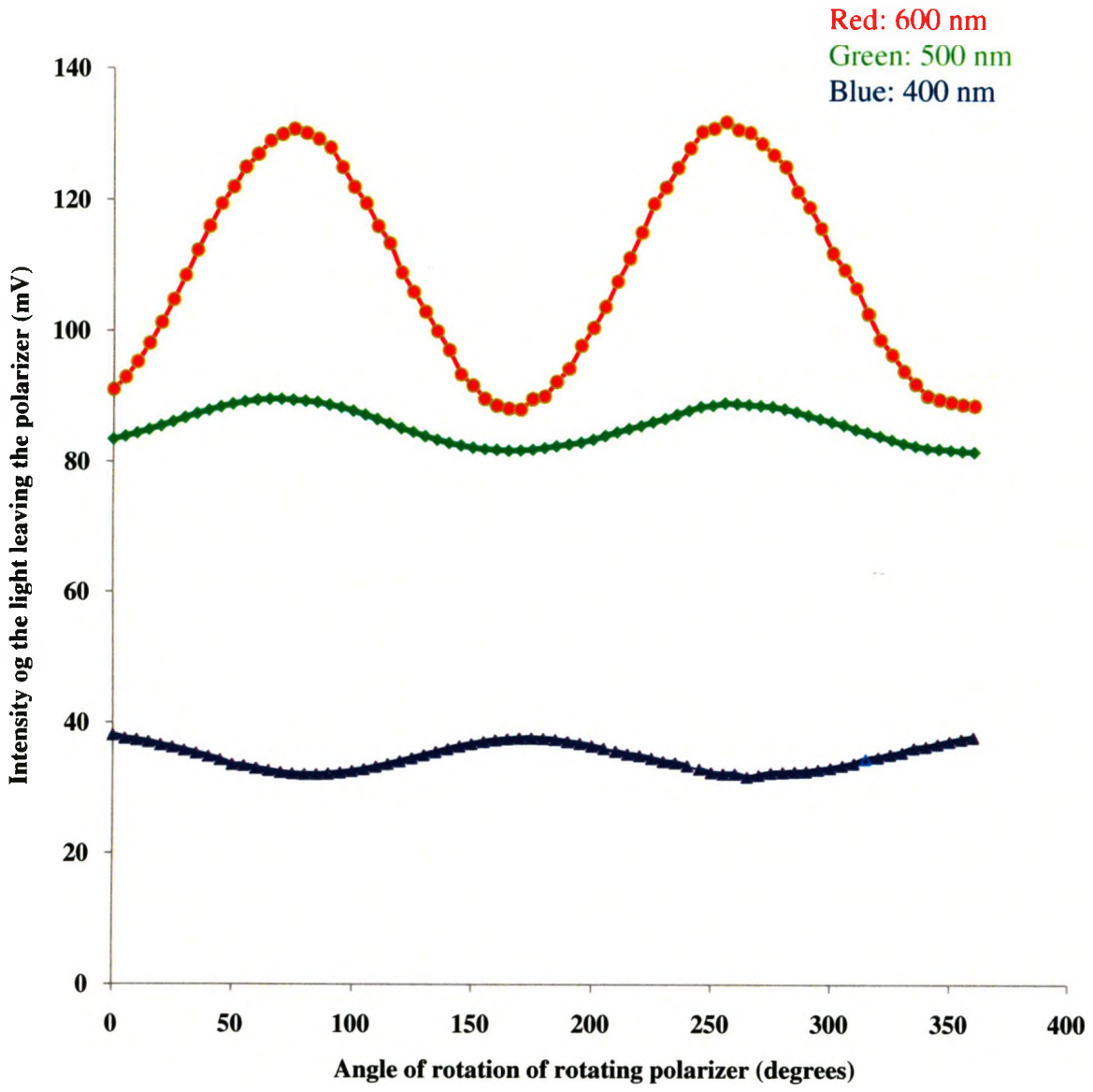

Figure 3.3. *Transmitted intensity behind the fiber entrance polarizer with respect to the polarization angle of the polarizer. Blue, green and red data sets are measured at 400, 500 and 600 nm, respectively.*

3.4. Temperature Stabilized Box

In order to test the home-made temperature stabilized box, described in chapter 2, a time dependent temperature measurement for a given set-temperature was measured.

Therefore a temperature sensitive detector inside the box was monitored and the heating bath circulator temperature was set to 27 °C. The heating curve is depicted in figure 3.4 implies that the inside temperature reaches a constant temperature of 25.5 °C after approximately 25 minutes.

As it was described in chapter 1, in collagen by increasing the temperature to 60 °C a systematic change in the optical rotatory spectrum with the denaturing process of collagen into gelatin happens. This phenomenon will be examined with spectral polarimeter setup. To gain the temperature-set of the bath circulator for box operation at 60 °C, a time dependent measurement was carried out for the box. It was observed that when the temperature of circulator bath reaches to 75.5 °C, it would be able to produce an environment with 60 °C inside the sample box. The temperature difference between the bath circulator and the box is a parameter that should be considered in the next experiments for realizing the accurate denaturation time. Figure 3.5 indicates that the temperature of the interior of the box reaches from 25.1°C to 60 °C after 50 minutes.

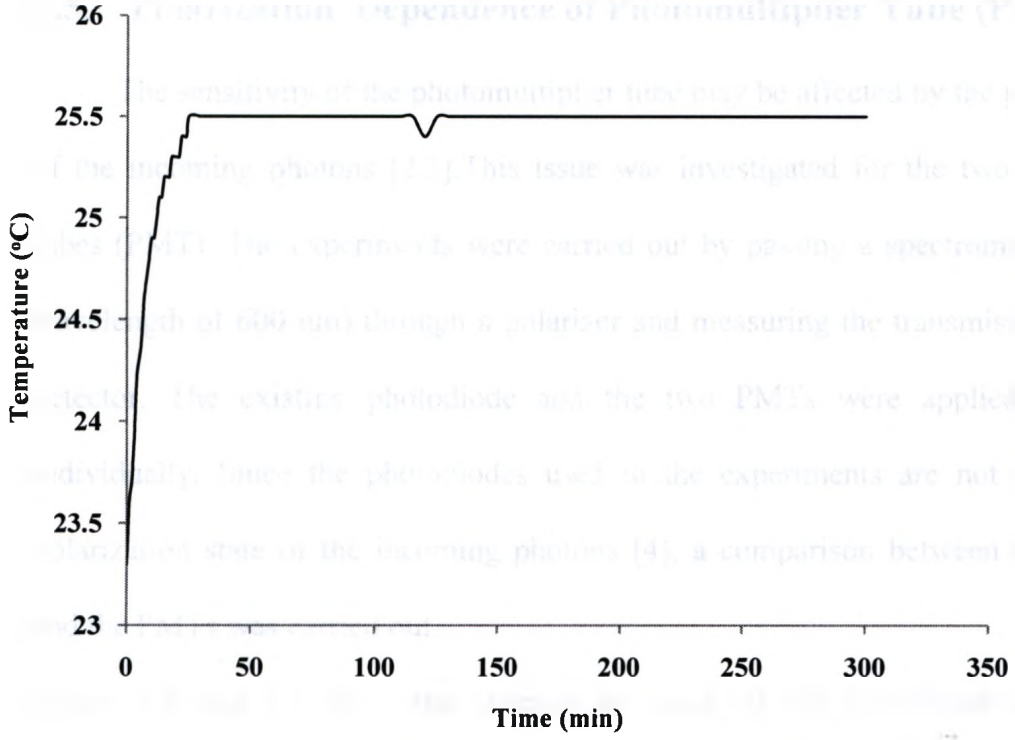

Figure 3.4. *Heating curve of the interior of the sample box . The temperature setting was chosen to be 27°C.*

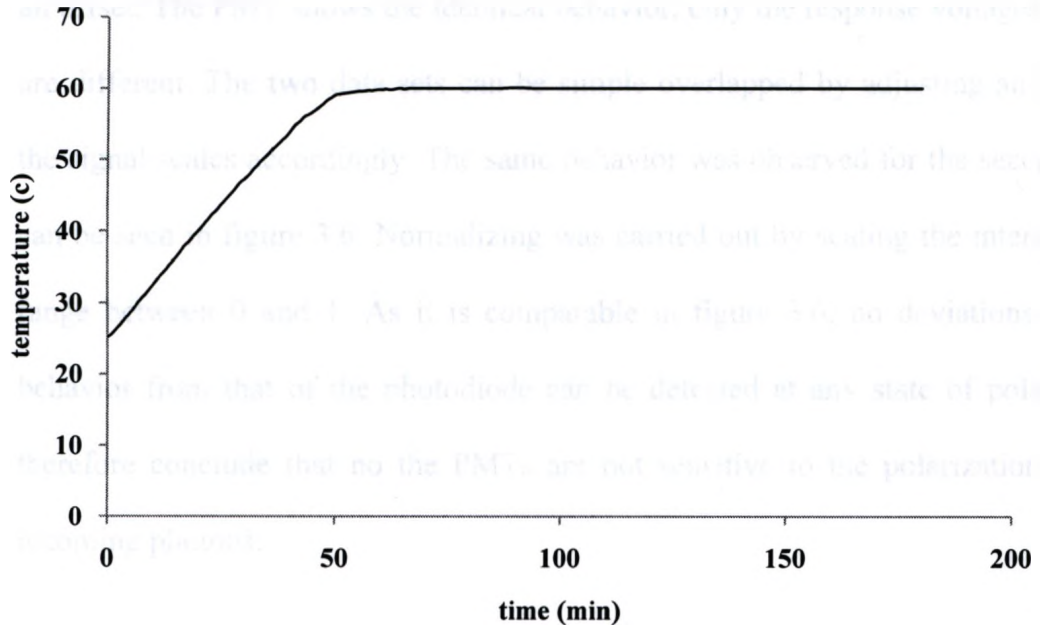

Figure 3.5. *Heating curve of the interior of the sample box from 25.1 °C to 60°C*

3.5. Polarization Dependence of Photomultiplier Tube (PMT)

The sensitivity of the photomultiplier tube may be affected by the polarization state of the incoming photons [2,3].This issue was investigated for the two photomultiplier tubes (PMT). The experiments were carried out by passing a spectrometer light (at the wavelength of 600 nm) through a polarizer and measuring the transmission light with a detector. The existing photodiode and the two PMTs were applied as a detector individually. Since the photodiodes used in the experiments are not sensitive to the polarization state of the incoming photons [4], a comparison between the photodiodes and the PMTs was carried out.

Figure 3.6 and 3.7 show the changes in signal of the photodiode and the PMTs, respectively at $\lambda = 600$ nm during scanning the rotating polarizer. As the light from the monochromator is partially polarized, the photodiode shows an oscillatory behavior with an offset. The PMT shows the identical behavior, only the response voltages of the signal are different. The two data sets can be simple overlapped by adjusting and normalizing the signal scales accordingly. The same behavior was observed for the second PMT as it can be seen in figure 3.6. Normalizing was carried out by scaling the intensity data to a range between 0 and 1. As it is comparable in figure 3.6, no deviations of the PMT behavior from that of the photodiode can be detected at any state of polarization. We therefore conclude that no the PMTs are not sensitive to the polarization state of the incoming photons.

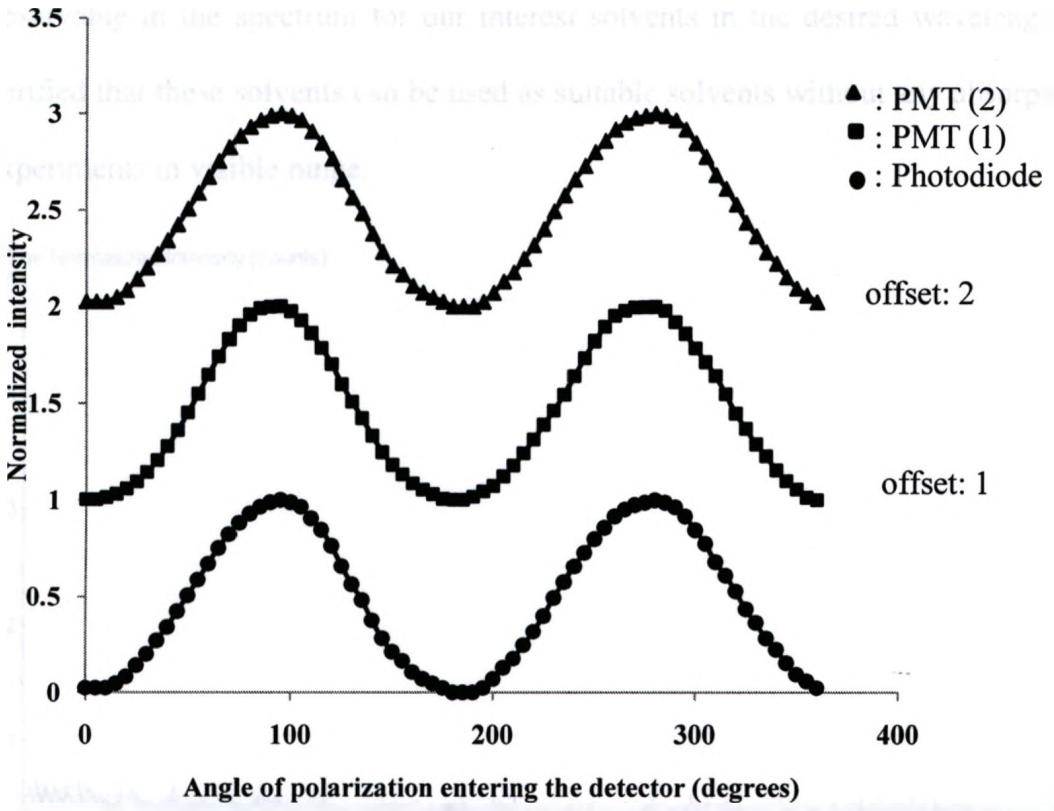

Figure 3.6. *Photodiode and two photomultipliers normalized signal versus angle of polarization.*

3.6. Transmission Spectrum of Solvents

Figure 3.7 shows the transmission spectrum taken for different solvents (refer to chapter 2). The spectrometer made possible to capture and store a full spectrum into memory every millisecond when the spectrometer is interfaced to a computer via a USB port. The same result was obtained for different lengths of fibers. The measurement of signals in optical spectrometry is influenced by the presence of spurious signals. The cause of these noise sources may be found in the light sources, the absorbing medium, the detectors, and the electronic measurement systems used in optical

spectrometry [5]. As it can be seen in the figure, No significant absorption peak is observable in the spectrum for our interest solvents in the desired wavelength range. It verified that these solvents can be used as suitable solvents without any absorption for our experiments in visible range.

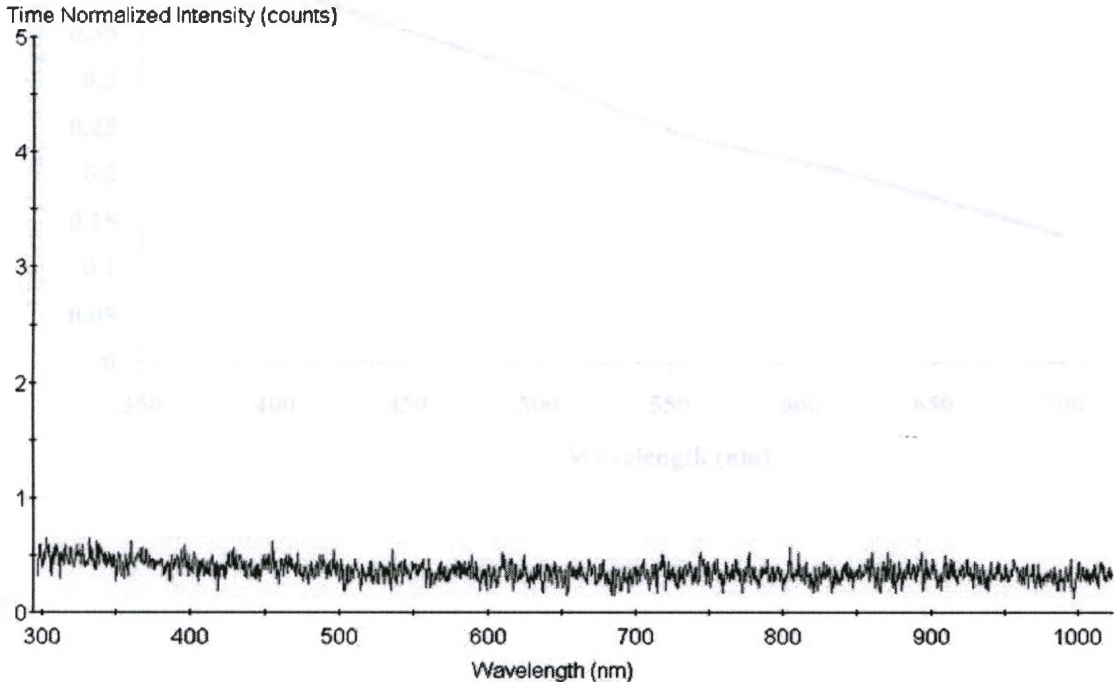

Figure 3.7. *Transmission spectrum of water, ethanol, toluene, benzene, isopropanol, ether, acetone and methanol in different length of silica and Teflon AF fiber.*

3.7. Investigation of Optical Rotatory Dispersion for Chiral Solutions

A solution of R-(+)-limonene dissolved in toluene with a concentration of 5 mM was prepared. Silica optical fibers at three different length of 28, 225.2 and 421.4 cm in the spectral polarimeter were filled with this solution. The monochromator was scanning at the range of 400-700 nm with a scanning speed of 1nm/s. To curl the long fibers, RAF figuration mentioned in previous chapters were applied. The angle of rotation was calculated by using the equation 2.4 mentioned in chapter 2 for different wavelength and the

results were plotted versus wavelength as it is shown in the figures 3.8.a,b and c.

a)

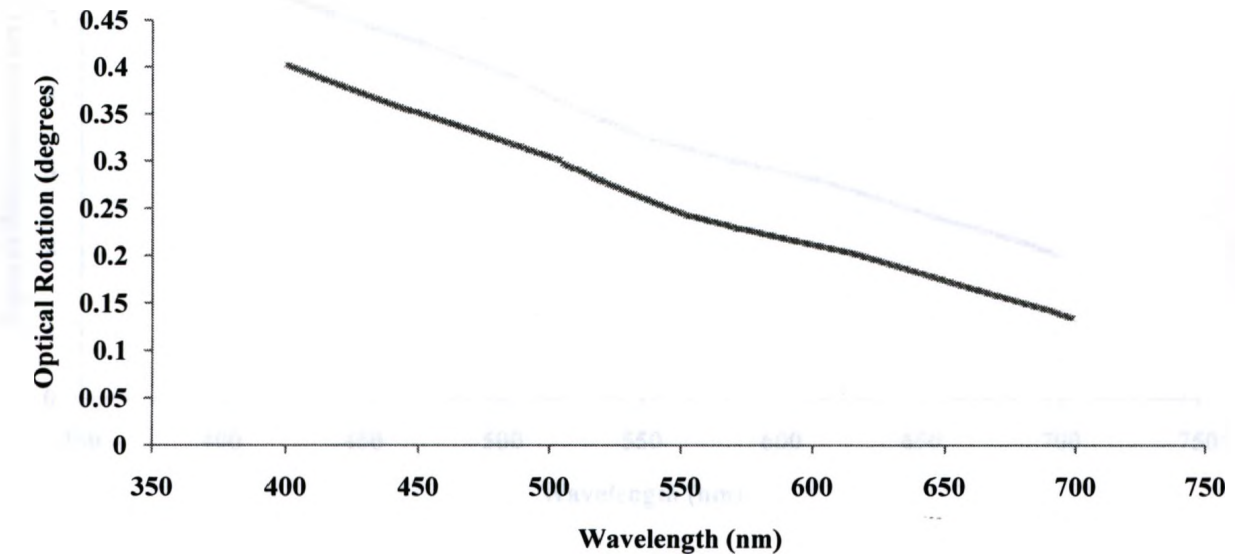

b)

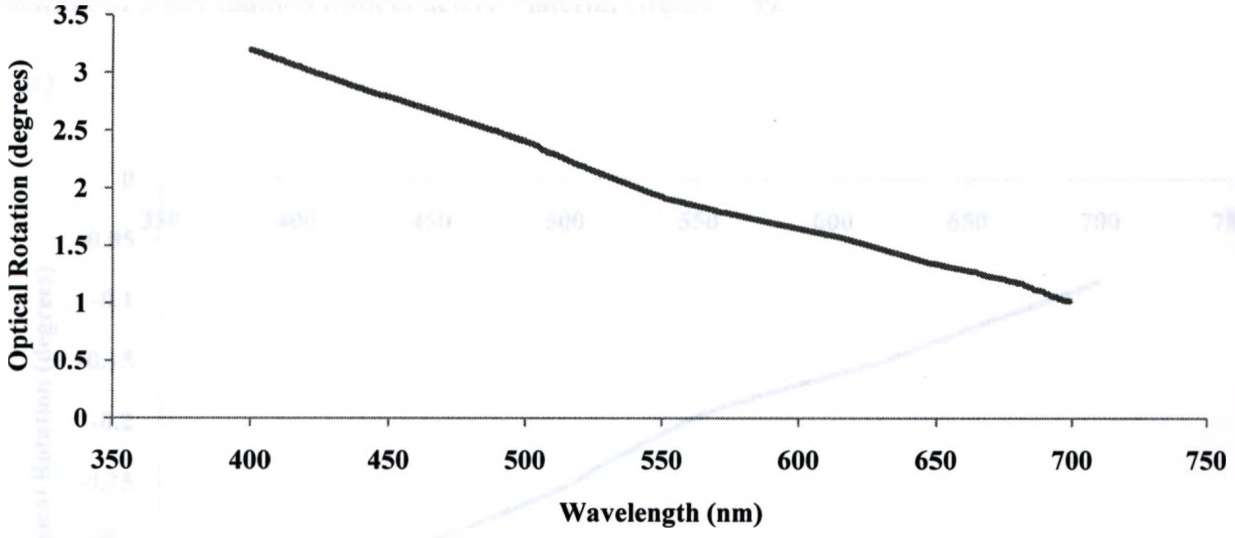

C)

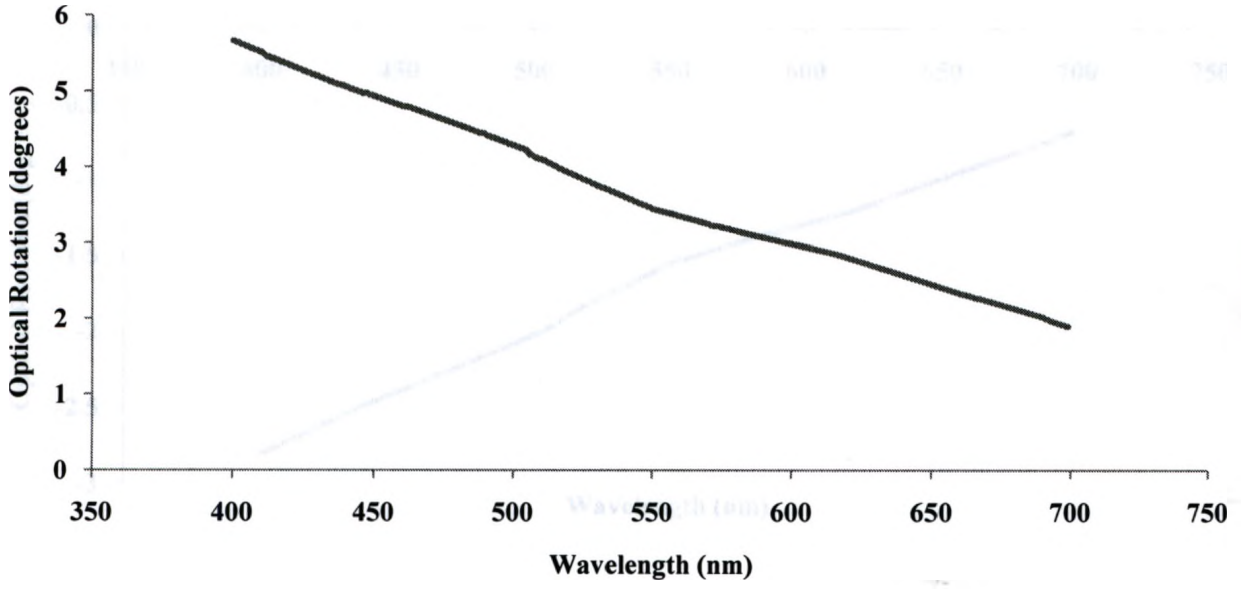

Figure 3.8. *Optical rotation dispersion measured with the spectral polarimeter for R-(+)-limonene (5mM in toluene)in silica hollow optical fiber at a) 28, b)225.2 and c) 421.4 cm length.*

These experiments were repeated for S-(-)-limonene solution to explore the optical rotation of a left-handed optical active material (figure 3.9).

a)

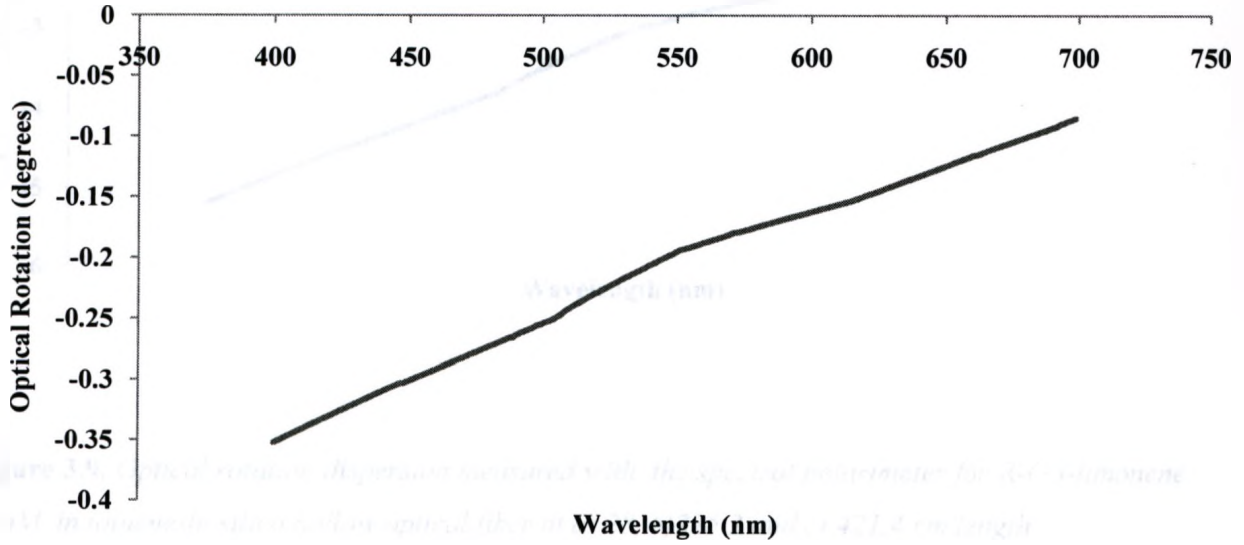

b)

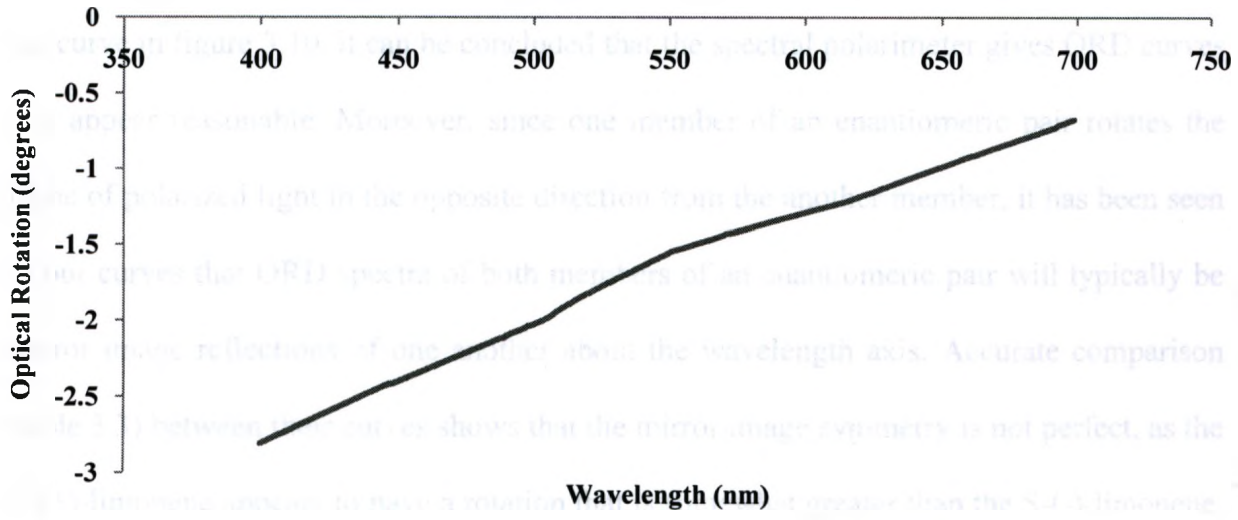

C)

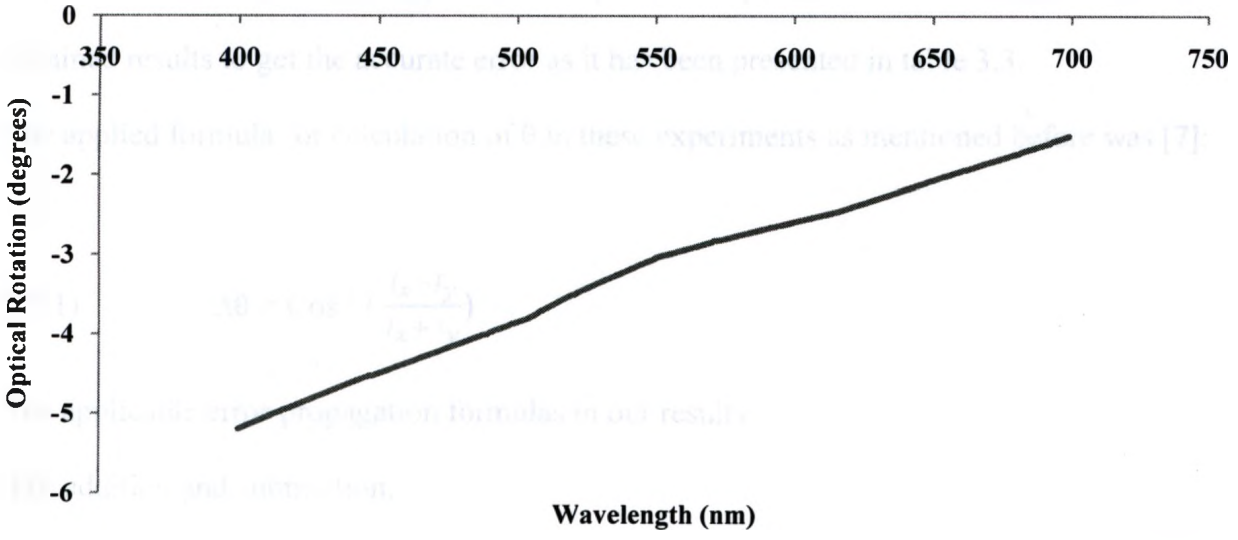

Figure 3.9. *Optical rotation dispersion measured with the spectral polarimeter for R-(+)-limonene (5mM in toluene)in silica hollow optical fiber at a) 28, b)225.2 and c) 421.4 cm length.*

As shown in figure 3.10, in a conventional spectral polarimetry, the ORD curves of a pair of enantiomers decrease with increasing wavelength [6]. By comparing figure 3.8.a to the curve in figure 3.10, it can be concluded that the spectral polarimeter gives ORD curves that appear reasonable. Moreover, since one member of an enantiomeric pair rotates the plane of polarized light in the opposite direction from the another member, it has been seen in our curves that ORD spectra of both members of an enantiomeric pair will typically be mirror image reflections of one another about the wavelength axis. Accurate comparison (table 3.3) between their curves shows that the mirror image symmetry is not perfect, as the R-(+)-limonene appears to have a rotation that is somewhat greater than the S-(-)-limonene. This comparison was carried out by selecting 7 different wavelength and comparing the optical rotation of R-(+)-limonene with S-(-)-limonene at those points. This asymmetry is accounted for the purity of chemicals [(R) 97 %, (S) 96 %] and the concentration of the prepared solutions, not the applied technique. Error propagation was calculated for the obtained results to get the accurate error as it has been presented in table 3.3.

The applied formula for calculation of θ in these experiments as mentioned before was [7]:

3.7.1) $$\Delta\theta = \mathrm{Cos}^{-1}\left(\frac{I_x - I_y}{I_x + I_y}\right)$$

The applicable error propagation formulas in our results:

For addition and subtraction,

3.7.2) $$\Delta z = \sqrt{(\Delta x)^2 + (\Delta y)^2 + \ldots}$$

Division formula,

3.7.3) $$\Delta z = z\sqrt{(\frac{\Delta x}{x})^2 + (\frac{\Delta y}{y})^2 + \ldots}$$

And $\cos^{-1}(\theta)$ formula,

3.7.4) $$\Delta z = \sqrt{(-\frac{x}{\sqrt{1-x^2}})^2 (\Delta x)^2 + (-\frac{y}{\sqrt{1-y^2}})^2 (\Delta y)^2 + \ldots}$$

For example for R-limonene at wavelength 400 nm, I_x and I_y were obtained: 2.7828$\pm$ 0.051 and 0.0274 $\pm$ 0.038. Putting them in above formulas achieved θ : 5.66 $\pm$ 0.032

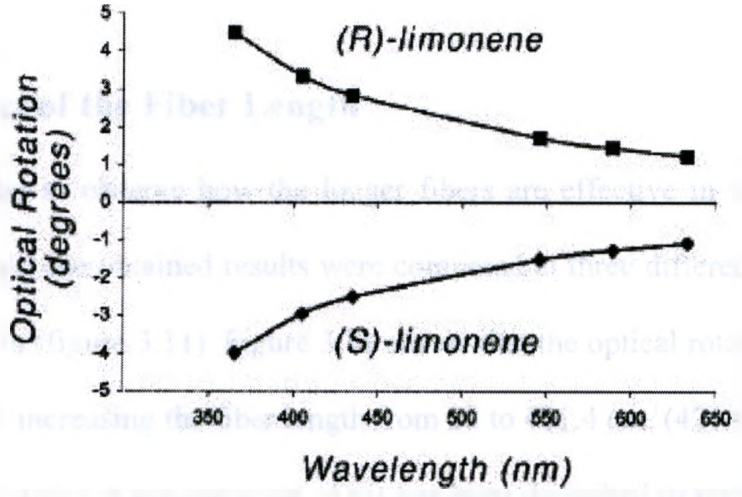

Figure 3.10. *Optical rotation (degrees) as a function of wavelength (nm) measured with polarimeter for R-(+)-limonene and (S)-(-)-limonene (Adopted from [6])*

Wavelength	Optical Rotation (degrees)	
	R-(+)-limonene	S-(-)-limonene
400	5.660 ± 0.032	-5.191 ± 0.065
450	4.931 ± 0.045	-4.492 ± 0.122
500	4.280 ± 0.218	-3.840 ± 0.056
550	3.440 ± 0.052	-3.031 ± 0.108
600	2.992 ± 0.156	-2.583 ± 0.074
650	2.451 ± 0.037	-2.052 ± 0.053
700	1.890 ± 0.048	-1.501 ± 0.066

Table 3.3. *A comparison of optical rotation data between R-(+)-limonene and S-(-)-limonene in 7 different wavelength for a 421.4 cm silica fiber*

3.8. Effect of the Fiber Length

In order to observe how the longer fibers are effective in the optical rotation of chiral materials, the obtained results were compared at three different wavelengths versus the fiber length (figure 3.11). Figure 3.11 shows that the optical rotation was increased up to 14 times by increasing the fiber length from 28 to 421.4 cm. (421.4/28 = 15) at the same concentration with a 6 percent error. As it has been described in previous chapters, this is based on the equivalence of interaction length to fiber length that highlights the potential for using a liquid-core waveguide in spectral polarimetry: as the length of the fiber is increased, sensitivity should increase proportionally [6,8].

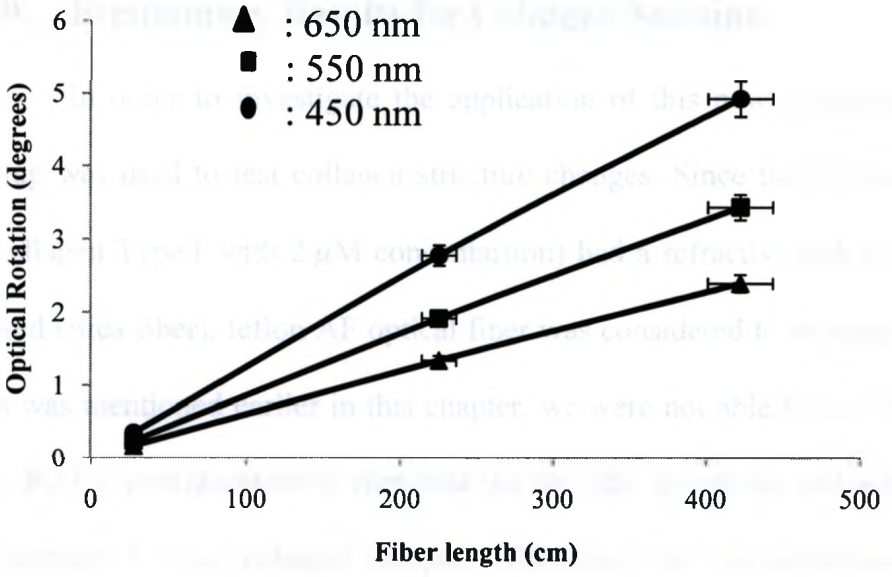

Figure 3.11. *Optical rotation of R-(+)-limonene at wavelengths of 450, 550 and 650 nm versus fiber length.*

As mentioned in chapter 2, concentration of solution is an effective parameter in calculation of optical rotatory dispersion of chiral molecules and limit of detection (LOD) can be defined as the sensitivity of setup. In order to calculate the limit of detection for this new spectral polarimeter, the following experiment was carried out. In a fixed fiber length, R-(+)-limonene concentration was decreased to the lowest level which still the curves with the same behavior as shown in figure 3.8 were achievable. After 25 measurements and diluting the solution, LOD were found 0.3 and 0.1 μM for a 220.4 and 428.8 cm fiber, respectively. Since the laser polarimetry setup showed a 0.3 mM LOD for a 2 m fiber, the new setup presented more that 3 orders of magnitude better due to implementation of PMT.

3.9. Preliminary Results for Collagen Solution

In order to investigate the application of this new polarimeter for proteins, the setup was used to test collagen structure changes. Since the prepared collagen solution (Collagen Type I with 2 μM concentartion) had a refractive index about 1.34 (less than fused silica fiber), teflon AF optical fiber was considered to be used as a sample cuvette. As was mentioned earlier in this chapter, we were not able to curl the teflon AF fiber in the RAF 8 configuration to eliminate the periodic deviations and achieve optical rotatory dispersion for our collagen samples. Therefore, the monochromator was fixed at the wavelength of 546 nm [9] for the experiments. First, a 202 cm teflon fiber filled with milli-Q water was curled in two loops laying in the same plane and the polarization changes were recorded as a reference curve. Then, the fiber was filled with collagen solution and the polarization changes were recorded at the same conditions. The next step was focused on the effect of temperature on the optical activity of proteins (refer to chapter 1). To aim this, the experiment was carried out when the temperature was increased to 60 ^{o}C. According to the results for the temperature stabilized box, the final measurement was carried out after 50 minutes. Figure 3.12 represents the obtained polarization curves. As it can be seen in the red curve in this figure, after filling the fiber with collagen solution, a shift in the polarization is observable due to the optical activity of collagen which changes the optical rotation of the polarized light for 4.13 $\pm$ 0.03 degrees. The polarization changes in green curve in compared with red one depicts clearly that by increasing the temperature, a decrease in the optical rotation curve (2.32 $\pm$ 0.04)is detectable with the denaturing process of collagen into gelatin at 60 ^{o}C that shows the same behavior according to the literature [9,10].

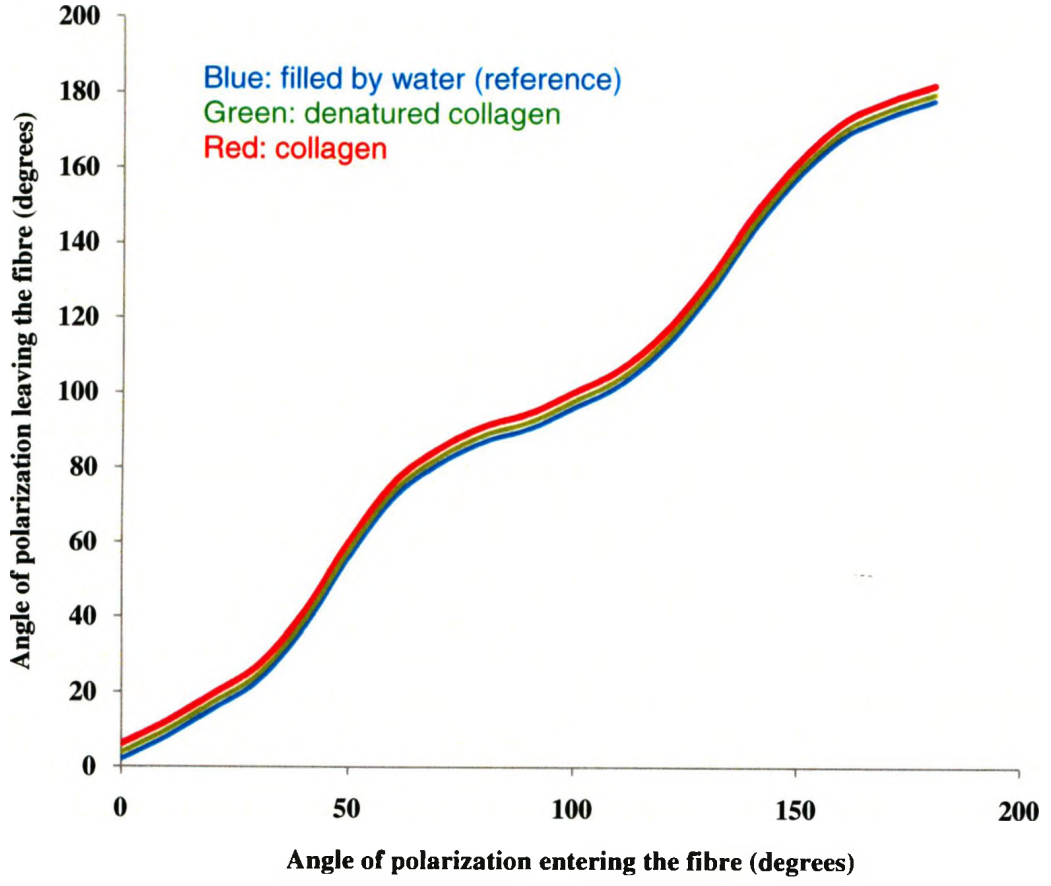

Figure 3.12. *Angle of polarization after passing through a teflon AF hollow optical fiber with 202 cm length at 546 nm. The fiber is curled in two loops in a same plane at a radius of 15.1 cm. Blue, red and green data sets are curves for fiber filled with milli-Q water, fiber filled with collagen at room temperature and fiber filled collagen(heated up to 60 °C) respectively.*

3.10. References

1. K. Rabinovitch, L. R. Canfield, and R. P. Madden, *A Method for Measuring Polarization in the Vacuum Ultraviolet*, Appl. Opt. **4**, 1005-1010 (1965).

2. S.A. Hoenig and A. Cutler AE, *Polarization sensitivity of the RCA 6903 photocathode tube*, appl. Opt. **5,6**, 1091 (1996).

3. H. Hora, *Experimental evidence of the angular dependence of electron excitation in photoemission,* Phys. Stat. Soli (a). **5** , 159 (1971).

4. Saito, M Yuri and H Onuki, *Polarization characteristics of semiconductor photodiodes,* Metrologia. **32**, 485 (1995).

5. C. TH. J. Alkemade and W. Snelleman, *A review and tutorial discussion of noise and signal-to-noise ratio in analytical spectrometry-I. Fundamental principles of signal-to noise ratios.*, Spectrochimica Acta. **33**, 383-399 (1978).

6. Carlos Calleja-Amador, Dennis H. Rabee, Kenneth W Busch, and Marianna A. Busch, *Novel Spectropolarimeter Empolying Fixed Polarizers for the Determination of Optically Active Samples*, Applied Spectroscopy. **62**, 402-413 (2008).

7. Vern Lindberg, *Uncertainties and error propagation Part I of a manual on uncertainties, graphing and the vernier caliper* (2000).

8. Fuwa,K., Wei Lei. Fujiwara, *Spectrophotometry with liquid-core optical fiber in aqueous solution phase in the ultraviolet region*, Annual. Chem. **56** (1984).

9. Wei Lei, Keiichiro Fuwa, Anal. Sci. **3** (1986)

10. Cohen,C. ,*Optical rotation and helical polypeptide chain configuration in collagen and gelatine,* Journal of Biophysics and biochemistry.**1** (1995).

11. G.S. Baht, G.K. Hunter, H.A. Goldberg *Bone sialo protein-collagen interaction promotesd hydroxyapatite nucleation*, , Matrix Biology **27**, G.S. Baht, G.K. Hunter, H.A. Goldberg (2008)

CHAPTER 4

SUMMARY AND OUTLOOK

4.1. Summary

The primary motivation of the work presented in this thesis was to ultimately develop a new highly sensitive fiber spectral polarimeter for application in protein structural detection.

Previously, in our group, a simple laser fiber polarimeter based on a liquid core hollow optical fiber waveguide had been demonstrated. Extremely small volumes (39 µl) with a light interaction length of 2.2 m were achieved. At 543.5 nm and 632.8 nm wavelength, emitted from two different lasers as light sources, the optical activity of small chiral molecules were determined with a very simple setup with 70-90 milli degree resolution and concentrations down to 10 mM, e.g. of limonene [1].

First, the fundamental liquid-core fiber polarimeter setup was applied to characterize the fibers in different length. Since many biological sample solutions are aqueous with a refractive index slightly above 1.33, teflon AF hollow optical fibers with a refractive index of 1.29 were introduced that can be applicable for water based samples. It was achieved that the fiber length for the silica and Teflon AF fiber could be extended up to 5 and 2 m, respectively.

In order to investigate the absorption issues of fibers filled with different solvents for application in the next experiments, a simple absorption spectroscopy setup operating in visible range was employed. It was confirmed that there is no absorption in the fibers for our interest solvents in the desired wavelength range.

The main focus of this thesis was to assemble a new spectral polarimetry setup based on the laser liquid-core fiber polarimeter technology in order to exploit the optical rotatory dispersion of chiral macromolecules. To gain the best efficiency from the

spectral polarimeter setup and optimize the function of it, each part was characterized and optimized individually. In order to use the monochromator as a light source with the highest possible transmission, the polarization state of the light leaving the spectrometer was investigated at three different visible wavelengths: 400, 500 and 600 nm. It was concluded that aligning the fiber entrance polarizer at an orientation of 75° would be the best choice to for launching the highest number of available photons over the entire wavelength regime.

Next, in order to test the home-made temperature stabilized box (refer to chapter 2) a time dependent temperature measurement for a stable room temperature (25 ^{o}C) and collagen denaturing temperature (60 ^{o}C) was measured and the desired heating curves were obtained.

To ensure the sensitivity of the photomultiplier tubes are not affected by the polarization state of the incoming photons, the two photomultiplier tubes (PMT) were investigated individually. This was done by making a simple comparison between the PMT and a standard photodiode. It was verified that the PMT is not sensitive to the polarization state of the incoming photons in the frequency range investigated.

In next step, the optimized setup was tested by some known chiral materials. It was proved that the spectral fiber polarimeter works properly and shows an improvement due to the enhanced sample interaction length. The optical rotatory dispersion of the chiral materials was investigated and compared with the literature. A detection resolution in order of microdegrees and a limit of detection (LOD) of 0.3 and 0.1 μM for a 220.4 and 428.8 cm fiber were achieved with this new spectral polarimeter.

Finally, this novel technology was employed to test collagen solution. It was carried out by using a 202 cm Teflon AF fiber at the wavelength of 546 nm for a 2 μM Type I collagen. The optical rotation changes were plotted for the sample in room temperature and 60 ^{0}C (denaturing temperature). An observable changes were detected after filling the fiber with protein solution and then heating it up to 60 ^{0}C due to the optical activity of collagen.

4.2. Outlook

By designing a new apparatus for holding the teflon fiber or characterizing new fibers which can be used in water-based solutions, this technology will be applicable in detecting the changes in the tertiary structure of proteins. It also will be able to investigate enzyme activity and their kinetics, when a change in chirality -leading to a change in the optical rotator dispersion - is coming along with it. The impact of this novel technology will be a better understanding in the kinetics of protein response to external stimuli and denaturing with respect to structure-function relationships.

The system can be tested with a very small vesicular system to determine the possibility to operate the fiber without scattering losses here. If this can be carried out successfully, transmembrane proteins will be incorporated into the vesicles. Activation induces structural changes in the transmembrane proteins [2] might be a possibility in order to apply the system to a new application.

Future possible research directions can be calcium-induced conformational changes, e.g. structural changes in parkin [3], a protein involved on parkinson disease upon interaction with targets.

4.3. References

1. T. C. Preston, S. Stille, N. D. Jones and S. Mittler, *Simple liquid-core waveguide polarimetry,* Applied Physics Letters. **89** (2006).

2. M. Clément, J. Cabana, B. J. Holleran, R.Leduc, G. Guillemette, P. Lavigne, E. Escher, *Activation induces structural changes in the liganded angiotensin II type 1 receptor,* , Journal of Biological Chemistry., **284** (39) (2007).

3. K.K. Dev, H. Van der Putten, B. Sommer and G. Rovelli, *parkin-associated protein and Parkinson's disease, Neuropharmacology.* **45** (2003)